Available online at www.sciencedirect.com

ScienceDirect

Geochimica et Cosmochimica Acta 169 (2015) 63–81

Geochimica et Cosmochimica Acta

www.elsevier.com/locate/gca

Silicon isotope systematics of acidic weathering of fresh basalts, Kilauea Volcano, Hawai'i

Steven M. Chemtob [a,b,*], George R. Rossman [a], Edward D. Young [c], Karen Ziegler [d], Fréderic Moynier [e], John M. Eiler [a], Joel A. Hurowitz [f]

[a] Divison of Geological and Planetary Sciences, California Institute of Technology, Pasadena, CA 91125, United States
[b] Department of Earth and Planetary Sciences, Washington University, St. Louis, MO 63130, United States
[c] Department of Earth, Planetary, and Space Sciences, University of California, Los Angeles, CA 90095, United States
[d] Institute of Meteoritics, University of New Mexico, Albuquerque, NM 87131, United States
[e] Institut de Physique du Globe de Paris, Institut Universitaire de France, Université Paris Diderot, Paris, France
[f] Department of Geosciences, Stony Brook University, Stony Brook, NY 11794, United States

Received 26 January 2015; accepted in revised form 20 July 2015; Available online 26 July 2015

Abstract

Silicon stable isotopes are fractionated by a host of low-temperature aqueous processes, making them potentially useful as a weathering proxy. Here we characterize the silicon isotope signature of surficial chemical weathering of glassy basaltic lava flows at Kilauea Volcano, Hawaii. Fresh basalt flow surfaces (<40 years old) frequently feature opaque amorphous silica surface coatings up to 80 μm thick. These silica coatings and associated silica cements are enriched in the heavier isotopes of Si ($\delta^{30}Si_{NBS\text{-}28} = +0.92‰$ to $+1.36‰$) relative to their basaltic substrate ($\delta^{30}Si_{NBS\text{-}28} = -0.3‰$ to $-0.2‰$). Secondary clays and opals are typically depleted in ^{30}Si relative to the dissolved reservoirs from which they precipitated, so this sense of isotopic fractionation is unusual. Mechanisms capable of producing isotopically heavy secondary minerals were explored by conducting batch alteration experiments on fresh basaltic glass. Batch acidic alteration of basalt glass in HCl, H_2SO_4, and HF produced silica-rich surface layers resembling the Hawaiian surface coatings. Differences in fluid chemical composition affected the direction and magnitude of Si isotope fractionation. Basalt leaching in HCl or H_2SO_4 produced ^{30}Si-enriched fluids ($1000 \ln \alpha_{precip\text{-}Si(aq)} \cong -0.8‰$) and ^{30}Si-depleted secondary silica layers. In contrast, HF-bearing experiments produced highly ^{30}Si-depleted fluid compositions ($1000 \ln \alpha_{precip\text{-}Si(aq)}$ up to $+8‰$). Larger isotopic fractionations were observed in experiments with lower fluid–rock ratios. In Hawaii, where altering fluids contain H_2SO_4 and HCl but minimal HF, high $\delta^{30}Si$ values for the silica coatings were likely achieved by Rayleigh fractionation. Aqueous ^{30}Si-enriched silica was released during incongruent basalt dissolution then subsequently transported and deposited from an evaporating solution at the flow surface. Our results indicate that (1) altering fluid chemistry and fluid–rock ratio impact the Si isotope signature of chemical weathering and (2) $\delta^{30}Si$ of solids produced by low temperature aqueous alteration may diverge sharply from watershed- or landscape-scale weathering trends.

1. INTRODUCTION

Chemical weathering exerts a fundamental control on the distribution of primary and secondary minerals observed at the Earth's surface. The rates and products of subaerial chemical weathering are strongly influenced by

* Corresponding author at: Department of Earth and Environmental Sciences, Temple University, Philadelphia, PA 19122, United States.
E-mail address: chemtob@temple.edu (S.M. Chemtob).

http://dx.doi.org/10.1016/j.gca.2015.07.026
0016-7037/

temperature, rainfall rates, and environmental chemistry (Raymo et al., 1988; Riebe et al., 2004; Das et al., 2005). Therefore, the development of geochemical and isotopic proxies for the mechanisms and intensity of weathering is of interest for deciphering climatic and environmental conditions in the geologic record.

Si stable isotopes are an increasingly prominent tool for probing the weathering history of modern and ancient low-temperature environments (Ding et al., 2004; Alleman et al., 2005; Ziegler et al., 2005; Georg et al., 2006, 2007; Bern et al., 2010; Cardinal et al., 2010; Opfergelt and Delmelle, 2012). Low-temperature processes, such as secondary mineral precipitation, silica adsorption, and plant uptake, are associated with large Si isotopic fractionations (Li et al., 1994; Milligan et al., 2004; Opfergelt et al., 2006; Geilert et al., 2014), while variations in $\delta^{30}Si$ in igneous rocks are observable but small (Douthitt, 1982; Savage et al., 2010, 2011). Dissolved Si in fresh surface waters has high $\delta^{30}Si$ values relative to source bedrock or sediment (De la Rocha et al., 2000; Ding et al., 2004; Georg et al., 2007; Cardinal et al., 2010). This isotopic fractionation is commonly interpreted as a signature of chemical weathering of silicate rocks and subsequent precipitation of secondary silicates, which tend to be ^{30}Si-depleted relative to associated dissolved Si. The Si isotope composition of soils ($\delta^{30}Si$ from $-2.7‰$ to $+0.2‰$; Ziegler et al., 2005; Bern et al., 2010; Opfergelt and Delmelle, 2012) reflects a range of fractionating processes, including weathering of primary phases, precipitation of clay minerals, adsorption of silica on Fe oxides and amorphous Al-hydroxides, and biological uptake of Si (Ziegler et al., 2005; Delstanche et al., 2009; Opfergelt et al., 2010; Oelze et al., 2014), as well as the input of wind-blown dust (Bern et al., 2010). Samples with particularly low $\delta^{30}Si$ values, such as pedogenic silcretes (as light as $\delta^{30}Si = -5.4‰$) may have undergone multiple cycles of dissolution and re-precipitation (Basile-Doelsch et al., 2005). Groundwater from the Navajo Sandstone aquifer, Nevada, spans the range of primary and secondary mineral $\delta^{30}Si$ values, potentially reflecting varying degrees of redissolution of secondary clays and silcretes (Georg et al., 2009). The precipitation of biogenic silica, incorporated into the shells of diatoms and radiolaria in marine environments and into plant phytoliths in terrestrial environments, also fractionates Si isotopes, with low $\delta^{30}Si$ incorporated into the biogenic precipitate (Opfergelt et al., 2006; Leng et al., 2009). These observed fractionations have allowed the use of silicon isotopes as a proxy for depositional processes in several geologic records, including siliceous diatoms over the period of the Last Glacial Maximum (De La Rocha et al., 1998), Precambrian oceanic cherts (Robert and Chaussidon, 2006; van den Boorn et al., 2010) and banded-iron formations (Steinhöfel et al., 2009, 2010; Heck et al., 2011; Chakrabarti et al., 2012).

Several factors complicate the interpretation of Si isotope compositions in natural samples. One complicating factor is that many of the above-mentioned low-temperature processes, including precipitation, adsorption on nanophase oxide particles, and biogenic uptake, all produce similar Si isotope signatures. In systems in which multiple fractionating processes operated simultaneously, attributing Si isotopic signatures to a single fractionating mechanism is difficult and frequently requires the application of additional geochemical tracers. Another unresolved issue is that isotopic fractionation factors associated with precipitation of clays and opals ($\alpha_{precip\text{-}aqueous} \equiv [(^{30}Si/^{28}Si)_{precip}/(^{30}Si/^{28}Si)_{aqueous}]$) are poorly constrained. Previous experimental and analytical studies have established fractionation factors ($1000 \ln \alpha_{precip\text{-}aqueous}$) ranging from $-0.7‰$ to $-3.5‰$ for the $^{30}Si/^{28}Si$ ratio, although this range is strongly affected by kinetic processes (Douthitt, 1982; Li et al., 1994; Milligan et al., 2004; Geilert et al., 2014, 2015). Si isotope fractionation factors are rate dependent (Oelze et al., 2014; Geilert et al., 2015). For Si adsorption on Fe- and Al-hydroxides, Oelze et al. (2015) reported a fractionation factor of $-3‰$ for kinetic isotope fractionation and $0‰$ for equilibrium. Organic and inorganic ligands have been shown to affect Si speciation, solubility and dissolution rate (Chen and Marshall, 1982; Ohman et al., 1991; Azaroual et al., 1997; Bai et al., 2009), but variations in isotopic behavior with aqueous speciation of Si have not been explored. Effective interpretation of $\delta^{30}Si$ compositions of ancient rocks requires continued study of the isotopic signature of weathering under different conditions in natural and experimental settings.

This study focuses on the Si isotope compositions of products of local-scale chemical weathering of fresh basalts at Kilauea Volcano on the island of Hawai'i, USA. Young Kilauean basalt flows frequently feature opaque surface coatings, up to 100 μm thick, composed largely of hydrous amorphous silica (Minitti et al., 2007; Chemtob et al., 2010). These coatings form over a period of days to years by interaction of near-surface basalt with volcanically-derived acidic fluids (Chemtob and Rossman, 2014). Similar acid-fog alteration processes have been proposed as the mechanism for silica and sulfate mineral genesis on the surface and near-surface of Mars (Tosca et al., 2004; Hurowitz et al., 2006). Thin Si-rich alteration layers are commonly observed products of silicate weathering in natural and experimental settings (Gordon and Dorn, 2005; Fulignati et al., 2006; Ruiz-Agudo et al., 2012; Hellmann et al., 2013). The mechanism of silica layer formation has been studied extensively and is most commonly attributed to interface-coupled dissolution-precipitation (Ruiz-Agudo et al., 2012; Hellmann et al., 2013). However, the immediate source of Si and the degree of Si mobility during coating formation in the Hawaiian environment is unresolved. Previous studies on Si isotope fractionation during basalt weathering have focused on the composition of dissolved Si in rivers draining basaltic watersheds (Georg et al., 2007) or on the composition of soil profiles developed on much older Hawaiian basalts (Ziegler et al., 2005; Bern et al., 2010). This is, to our knowledge, the first study of Si isotope fractionation of *in situ* incipient basalt alteration products.

Additionally, this study presents laboratory experiments to determine the chemical and Si isotopic signature of leaching of Hawaiian basaltic glass by acids of relevance to the volcanic environment (H_2SO_4, HCl, HF). Previous basalt alteration experiments with similar experimental

setups (Oelkers and Gislason, 2001; Gislason and Oelkers, 2003; Tosca et al., 2004; Hurowitz et al., 2005) included no isotopic analysis of solid or liquid products. Our results indicate that Si speciation during chemical weathering exerts a major effect on the direction and magnitude of δ^{30}Si fractionation.

2. SAMPLE LOCALES AND DESCRIPTIONS

Silica-coated samples were collected from lava flows of various ages and locations proximal to Kilauea's Southwest Rift Zone (SWRZ) and East Rift Zone (ERZ) (Table 1). These localities are described in detail elsewhere (Chemtob et al., 2010; Chemtob and Rossman, 2014). Samples PU-009 and PU-010 are lavas emplaced in 1998 and collected in July 2010 on the northeast rim of Pu'u O'o, a basaltic cone on the ERZ. The subaerial and underside surfaces of these lavas are covered by a bluish-white coating, 30–80 μm thick, composed primarily of hydrous amorphous silica (Chemtob et al., 2012) and containing >90 wt% SiO_2 (Fig. 1a–c; Table S2). Infrared and ^{29}Si nuclear magnetic resonance spectroscopy of the PU-009 silica coating indicate it contains high concentrations of structural hydroxyl (5.5 wt%) (Chemtob et al., 2012). Samples KD-003, KD-005 and EA-30 were collected from coated spatter ramparts and pahoehoe toes erupted in 1974 in the Ka'u Desert along Kilauea's SWRZ, roughly 5 km downwind of Halema'uma'u Crater (Fig. 1d). Samples from the same locality were described in Chemtob et al. (2010).

Amorphous silica is observable at Kilauea not only as coatings on fresh basalts, but as cement in soils and regoliths (Seelos et al., 2010; Ziegler et al., 2010). The region near the south rim of Halema'uma'u Crater features a number of man-made soil berms, bulldozed by the U.S. military during World War II. These piles have since developed a ~1 cm indurated rind; samples of these rinds (S-12-41) were collected in April 2012 by Don Swanson. Scanning electron microscopy and infrared spectroscopic analyses of the cements indicates they are composed primarily of gypsum and amorphous silica (Fig. 1e). Amorphous silica cements were scraped and collected for analysis.

A sample of fresh basaltic glass (KP-fresh) was collected in July 2010 for use in alteration experiments from an active lava channel sourced at the Episode 58 vent, ~1 km east of Pu'u O'o. The collection site was roughly 7 km southeast of the source vent. The basalt is tholeiitic, highly vesicular and composed largely of glass, with ~10% phenocrysts (primarily plagioclase of composition An_{71}, with rare olivine), and is unaffected by aqueous alteration (Fig. 1f and g). The chemical composition of KP-fresh as determined by electron microprobe analysis is given in Table S2.

3. METHODS

3.1. Basalt dissolution experiments

Basalt dissolution experiments were carried out with a variety of acids and over a range of fluid–rock mass ratios (F/R) (Table 2). All experiments utilized KP-fresh glass, ground, sieved to a grain size fraction of 300–600 μm, and ultrasonicated to remove clinging fine particles. The "B-HCl", "B-HF", and "B-H_2SO_4" experimental series were batch experiments conducted in screw-top Savillex PFA vials using 0.1 M HCl, 0.1 M HF, and 0.1 M H_2SO_4, respectively. These acids were chosen because they represent the major acidic components of Hawaiian volcanic fumes (Greenland et al., 1985; Gerlach, 1993). Because our modeling results suggested variation in Si speciation with hydrofluoric acid concentration, additional experiments were conducted using 1 M HF. The vials were heated to 60 °C for periods ranging from 3 to 30 days. In some experiments, fluid samples were only collected at the experiment conclusion; in others, vials were periodically opened for fluid collection using an adjustable volume syringe. Fluid samples were small in volume (50–100 μL) and were diluted in 18.2 mΩ cm H_2O after collection. A subset of these fluids was selected for determination of silicon isotope composition. In select experiments, altered basalt gravel was collected and prepared for morphologic analysis. Fluid samples are labeled in this manuscript by the following convention: (series).(experiment letter).(sample #) (e.g., B-HCl.A.1 is the first fluid collected from experiment B-HCl.A).

3.2. Analytical methods

Solid samples were mounted in Petropoxy resin and polished for morphological analysis using alumina and

Table 1
Hawaiian basalt and silica sample descriptions.

Sample code	Sample description	Collection date	Age at collection	Figures
PU-009	Silica coated volcanic bombs, collected at rim of Pu'u O'o cone, East Rift Zone	August 2010	<13 years	1a and b
PU-010	Hollow pahoehoe shells with silica coatings on exposed side and underside, rim of Pu'u Cone	August 2010	13 years	1c
KD-003	Basaltic spatter rampart with prominent coatings, Ka'u Desert, Southwest Rift Zone	July 2010	36 years	1d
KD-005	Interior of coated pahoehoe flow, 1974 eruption, Ka'u Desert, Southwest Rift Zone	July 2010	36 years	None
KP-fresh	Fresh glass, episode 58 eruption, collected ~1 km east of Pu'u O'o	August 2010	Fresh	1f and g
S-12-41	Silica-indurated ash deposit, 1 cm thick, near south rim of Halema'uma'u Crater	April 2012	~ 60 years	1e

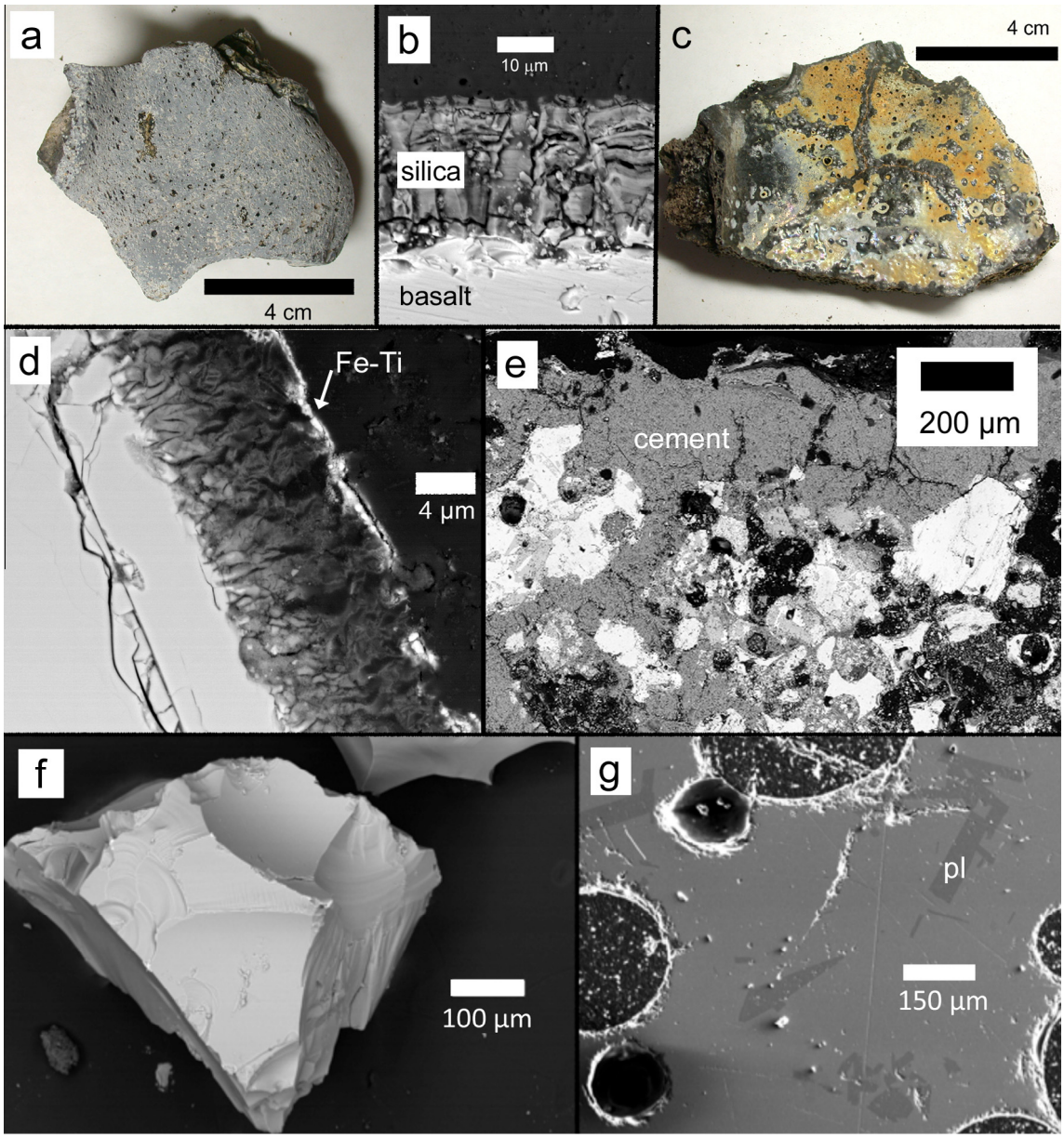

Fig. 1. Optical and backscattered electron (BSE) images of Hawaiian samples. (a) Sample PU-009, silica-coated volcanic bomb from the rim of the Pu'u O'o cone. (b) BSE image of cross-section of silica coating covering PU-009. The dark region at the top of the image is epoxy. (c) Coated underside of PU-010, a 2 cm thick pahoehoe shell from the rim of Pu'u O'o. (d) Cross-sectional BSE view of KD-003, a 1974 lava from Kilauea's Southwest Rift Zone. Coatings at this location feature a 1 μm layer of Fe-Ti oxide (marked by arrows). (e) BSE image of polished cross section of indurated ash sample S-12-41. Abundant gray-colored material is amorphous silica cement. Bright grains are basaltic glass. Dark regions are void space, carbonaceous material, or epoxy. (f) Secondary electron image of grains of KP-fresh, basalt glass collected from an active lava flow near Kalapana in 2010, as used for dissolution experiments. (g) Secondary electron cross-sectional view of KP-fresh. KP-fresh is highly vesicular and mostly glassy, with plagioclase laths (labeled "pl"). Dark material inside vesicles is epoxy.

diamond polishing papers. Backscattered electron images were collected with a LEO 1550 VP field emission scanning electron microscope (SEM) at Caltech, operating at 15 kV accelerating voltage and 10 mm working distance. An Oxford Inca X-ray energy dispersive spectrometer (EDS) was used for concurrent elemental analyses and for elemental mapping. Major and minor element compositions of Hawaiian silica coatings, basalts, and select experimental products were acquired by electron probe microanalysis (EPMA), using a JEOL JXA-8200 electron probe at Caltech. Concentrations of dissolved Si, Ti, Al, Mg, Ca, Fe, Mn, Na, K, P, and S in experimental fluid samples were determined using a Thermo iCap 6300 radial view inductively coupled plasma optical emission spectrometer (ICP-OES) at the Jet Propulsion Laboratory. Multielement standard solutions were prepared at concentrations of 0.1, 1, 10, and 50 mg/L. Samples and standards were acidified in 2% HNO_3.

Table 2
Summary of batch alteration experimental conditions.

Experiment	Apparatus	Fluid composition	T (°C)	Duration (days)	Basalt mass (g)	Initial fluid (mL)	Fluid–rock ratio	Fluid collection procedure
Batch HCl experiments								
B-HCl.A	PFA vial	0.1 M HCl	60	30	0.625	1.25	1.9	Periodic
B-HCl.B	PFA vial	0.1 M HCl	60	30	0.312	2.96	9.5	Periodic
B-HCl.C	PFA vial	0.1 M HCl	60	30	0.117	11.42	97.6	Periodic
B-HCl.D	Centrifuge tube	0.1 M HCl	60	3	1.002	0.3	0.3	Only at conclusion
B-HCl.E	PFA vial	0.1 M HCl	60	7	0.99	10.04	10	Periodic
Batch HF experiments								
B-HF.A	PFA vial	1 M HF	60	16	0.102	1.02	10	Periodic
B-HF.B	PFA vial	1 M HF	60	16	0.106	1.06	10	Only at conclusion
B-HF.C	PFA vial	1 M HF	60	16	0.242	0.725	3	Periodic
B-HF.D	PFA vial	1 M HF	60	16	0.242	0.726	3	Only at conclusion
B-HF.E	PFA vial	1 M HF	60	7	0.100	0.998	10	Only at conclusion
B-HF.F	PFA vial	0.1 M HF	60	7	0.100	0.996	10	Only at conclusion
B-HF.G	PFA vial	0.1 M HF	60	6	0.982	10	10	Periodic
Batch H_2SO_4 experiments								
B-H_2SO_4.A	PFA vial	0.1 M H_2SO_4	60	7	1	10	10	Periodic

Silicon isotope compositions were determined using a Thermo Finnigan Neptune multiple-collector inductively coupled plasma-source mass spectrometer (MC-ICP-MS) at University of California, Los Angeles (UCLA) and a Neptune Plus MC-ICP-MS at Washington University (WU). Silica coatings and cements were scraped from their basalt substrates using dental tools and purified by manual picking and magnetic separation.

For measurements at UCLA, sample digestions were performed following the methods of de la Rocha et al. (1996) and Ziegler et al. (2010). Silica samples, basaltic substrates, and standards were dissolved in 2.5 M ultrapure HF at 120 °C in sealed PFA screw-cap vials. The volume of HF added was proscribed by the Si concentration of the sample such that the final concentration of fluosilicate ions is below the threshold required for volatilization of SiF_4 gas. In some digestions, equal volumes of ultrapure HNO_3 were added to accelerate dissolution. For measurements at Washington University, sample digestions were performed following the HF-free method of Georg et al. (2006). Approximately 10 mg of solid sample and 200 mg NaOH flux were added to a silver crucible, then heated in a muffle furnace at 720 °C for 12 min. The resulting fusion cake was dissolved in 18.2 mΩ H_2O and acidified to 1% v/v HNO_3.

Purification of Si from digestions was achieved by ion-exchange chromatography. Fresh ion exchange columns were loaded with 2 mL of BioRad cation exchange resin DOWEX 50 W-X12 (200–400 mesh). The resin retains cationic species, but Si species do not bind to the resin. This purification method has been demonstrated in previous studies to achieve complete Si yield (Shahar et al., 2009; Ziegler et al., 2010). At UCLA, after cleaning the resin with distilled HCl, HNO_3, and 18.1 mΩ H_2O, columns were loaded with 3.6 μg Si in 0.02% HF and eluted with 6 mL of 18.1 mΩ H_2O, producing Si-purified solutions with concentrations close to 0.5 mg/L Si. HF concentrations in the final purified solutions are 0.0023%, low enough not to cause signal instability or matrix effects during MC-ICP-MS analysis (Shahar et al., 2009). At WU, after cleaning the resin as described in Savage and Moynier (2013), 30 μg Si in HF-free solution was loaded on the column and eluted with at least 5 mL of 18.1 mΩ H_2O, producing Si-purified solutions with concentrations close to 3 mg/L Si. Si-purified samples were acidified to 1% v/v HNO_3.

At UCLA, purified solutions were run on the Neptune MC-ICP-MS in dry plasma mode using the Cetac Aridus I desolvating system, the Cetac PFA microconcentric Aspire nebulizer, and a PFA spray chamber. The ions $^{28}Si^+$, $^{29}Si^+$, and $^{30}Si^+$ were all measured simultaneously. Ion beam intensities for experimental solutions were typically around 3.0 V for $^{28}Si^+$, 160 mV for $^{29}Si^+$, and 110 mV for $^{30}Si^+$. The MC-ICP-MS was operated at a mass resolving power (MRP) of ~9500, calculated for 5% of signal intensity. The bracketing standard solution was silica sand NBS-28 digested in dilute HF as described previously. Samples and standards were diluted to match peak heights to within 5–10%. Corrections for instrumental mass bias were performed by sample-standard bracketing. Long-term external reproducibility of the $\delta^{30}Si$ compositions of in-house standards (IRMM-018a, Diatomite, and "Big Batch") is <0.1‰ (Ziegler et al., 2010). The Neptune Plus MC-ICP-MS at WU was operated in medium-resolution mode (MRP = 7000) with conditions as described in Savage and Moynier (2013) and Pringle et al. (2013). Typical ion beam intensities were 7.0 V for ^{28}Si, 350 mV for $^{29}Si^+$, and 250 mV for $^{30}Si^+$. Reproducibility of NBS-28 using adjacent bracketing was <0.10‰ (Savage and Moynier, 2013). The method was validated by measurements of interlaboratory standards BHVO-2, Rose Quartz Mine quartz (RSQ), and Diatomite basalt standard; derived $\delta^{30}Si$ values for those

standards (Table 3) matched previously reported values (Reynolds et al., 2007; Chmeleff et al., 2008; Armytage et al., 2011; Savage et al., 2011).

Some of the Hawaiian silica samples contain sulfate, a species not retained by the resin, up to SO_4^{2-}/Si mass ratios of 0.035 (Chemtob et al., 2010). Sulfate and other oxyanions have been demonstrated to induce a mass bias on silicon isotope measurements (Hughes et al., 2011). To test the effect of sulfate on silicon isotope measurements in our study, we measured δ^{30}Si of NBS-28 standard solutions spiked with $(NH_4)_2SO_4$ standard solution, up to SO_4^{2-}/Si ratios of 1. At sulfate concentrations corresponding to the natural silica samples, the isotope bias was less than 0.1‰. The fluid from one alteration experiment, B-H_2SO_4, had high sulfate content (SO_4^{2-}/Si = 0.55; Table S3). This fluid was evaporated and the precipitate was fused in NaOH at 720 °C, volatilizing the sulfate component as SO_2. The fused precipitate was then digested in HNO_3 and analyzed for δ^{30}Si at WU as previously described.

Variations in Si isotopes are represented by the standard delta notation as δ^{30}Si or δ^{29}Si, defined as the deviation in per mil (‰) of the isotope ratio of the sample relative to that of the standard reference material (NBS-28), as follows:

$$\delta^{30}Si = [\{^{30}Si/^{28}Si\}_{sample}/\{^{30}Si/^{28}Si\}_{standard} - 1] \times 1000;$$

$$\delta^{29}Si = [\{^{29}Si/^{28}Si\}_{sample}/\{^{29}Si/^{28}Si\}_{standard} - 1] \times 1000.$$

We discuss the Si isotope data primarily in terms of δ^{30}Si values which are approximately twice that of δ^{29}Si. Δ^{29}Si represents the deviation in per mil (‰) from mass-dependent fractionation, as follows:

$$\Delta^{29}Si \equiv [1/m] \cdot \delta^{30}Si - \delta^{29}Si$$

where m is the kinetic mass-dependent fraction action slope (Young et al., 2002). Values of Δ^{29}Si were typically 0 ± 0.10‰. Mass-independent Si isotope fractionation is not expected in these systems, so Δ^{29}Si values near zero indicate interference-free measurements.

4. RESULTS

4.1. Silicon isotope analyses

4.1.1. Hawaiian basalts

Si isotope compositions of the Hawaiian basalts are listed in Table 3. Measured values of δ^{30}Si composition of the Pu'u O'o-derived basalts KP-fresh (-0.18 ± 0.19‰; 2 s.d., $n = 15$) and PU-009 (-0.11 ± 0.30‰; $n = 5$) are somewhat higher than values typically reported for basalts (Douthitt, 1982; Savage et al., 2010). Recent compilations indicate that average mid-ocean ridge basalt has $\delta^{30}Si = -0.27 \pm 0.06$‰ and average ocean island basalt has $\delta^{30}Si = -0.28 \pm 0.06$‰ (2 s.d.) (Savage et al., 2010, 2014). Our analyses of Pu'u O'o basalt PU-010 ($\delta^{30}Si = -0.26 \pm 0.17$‰) are consistent with these earlier basalt studies while our measurements of PU-009 and

Table 3
MC-ICP-MS silicon isotope analyses of standards, Hawaiian basalts and Hawaiian silica coatings and cements.

Sample	Lab	δ^{29}Si	2 s.d.	2 s.e.[a]	δ^{30}Si	2 s.d.	2 s.e.	n[b]
Standards								
RSQ quartz	UCLA	−0.02	0.10	0.05	0.02	0.16	0.08	4
Diatomite	WU	0.60	0.15	0.07	1.23	0.08	0.03	5
Basalts								
KP-fresh								
Analysis 1	UCLA	−0.04	0.11	0.05	−0.19	0.11	0.04	6
Analysis 2	UCLA	−0.06	0.09	0.05	−0.10	0.08	0.04	4
Analysis 3	WU	−0.14	0.20	0.09	−0.25	0.31	0.14	5
Average		−0.08	0.14	0.04	−0.18	0.19	0.05	15
KD-005 basalt	UCLA	−0.46	0.13	0.05	−0.84	0.10	0.04	6
PU-009 basalt	UCLA	−0.10	0.12	0.05	−0.11	0.30	0.13	5
PU-010 basalt								
Analysis 1	UCLA	−0.17	0.08	0.03	−0.25	0.30	0.12	6
Analysis 2	WU	−0.14	0.05	0.02	−0.27	0.15	0.06	6
Average		−0.15	0.05	0.01	−0.25	0.17	0.05	12
Silica coatings and cements								
PU-009 coating								
Analysis 1	UCLA	0.82	0.07	0.03	1.36	0.11	0.05	6
Analysis 2	UCLA	0.65	0.16	0.08	1.02	0.17	0.09	4
Analysis 3	WU	0.52	0.22	0.10	0.83	0.38	0.17	5
Analysis 4	WU	0.52	0.23	0.10	0.80	0.34	0.15	5
Average		0.65	0.09	0.02	1.06	0.14	0.03	21
PU-010 coating	UCLA	0.50	0.16	0.05	1.07	0.10	0.03	9
KD-003 coating	UCLA	0.47	0.08	0.03	0.92	0.10	0.04	6
S-12-41 cement	UCLA	0.59	0.11	0.05	1.10	0.12	0.06	5

[a] Standard error.
[b] Number of analyses.

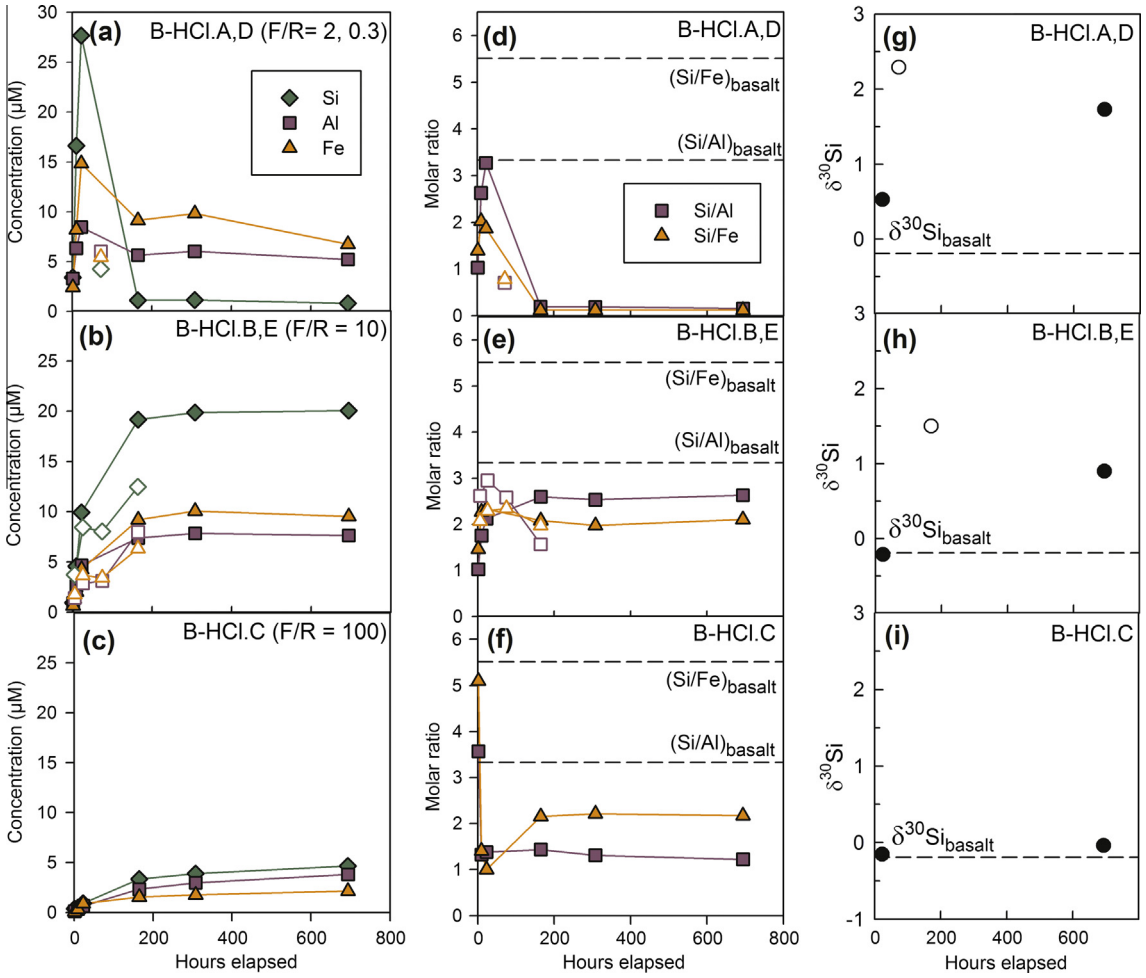

Fig. 2. Elemental concentrations (a–c), elemental molar ratios (d–f), and Si isotope compositions (g–i) of fluids from batch HCl alteration experiments. In molar ratio figures (d–f), dashed lines indicate the molar ratio of Si/Fe and Si/Al in KP-fresh basalt glass. In Si isotope figures (g–i), the dashed line indicates the δ^{30}Si of KP-fresh. (a), (d), and (g) depict experiments B-HCl.A (filled symbols; fluid/rock ratio = 2) and B-HCl.D (open symbols; fluid/rock = 0.3). (b), (e), and (h) depict experiments B-HCl.B (filled symbols) and B-HCl.E (open symbols) (both water/rock = 10). (c), (f) and (i) depict experiment B-HCl.C (fluid/rock = 100).

KP-fresh are high by ~0.10–0.20‰. Individual igneous systems may have more primary variability in Si isotope composition than previously suggested. Heterogeneity in Si isotope composition among basalts may be attributable to varying degrees of phenocryst crystallization and fractionation (Savage et al., 2011, 2014). Specifically, fractional crystallization of olivine and pyroxene drives basaltic melt towards isotopically heavier compositions (Savage et al., 2011). Although all purified solutions revealed negligible concentrations of relevant dissolved cations, it cannot be entirely ruled out that rare matrix effects caused this slight offset. In all cases, the difference between our PU-009 basalt data and previously published basalt data is much smaller than the differences between the weathering products and the basalt substrates of interest here.

A single basalt sample, KD-005, is ^{30}Si-depleted ($\delta^{30}Si = -0.84 \pm 0.10$‰) compared to previously reported basalt compositions. This basalt, erupted in 1974, has potentially undergone more extensive weathering processes than the younger ERZ lavas.

4.1.2. Hawaiian alteration materials

All MC-ICP-MS analyses of Hawaiian silica coatings and cements had ^{30}Si-enriched compositions relative to Hawaiian basalt (Table 3). Silica coatings of the basalt sample PU-009 were dissolved and analyzed four times, resulting in measurements of δ^{30}Si ranging from 0.80 ± 0.34‰ to 1.36 ± 0.11‰. This considerable inter-analysis variability is attributed to heterogeneity in the sample. Silica coatings from other basalt surfaces (PU-010, KD-003) and the silica cement S-12-41 had δ^{30}Si from 0.92 ± 0.10‰ to 1.10 ± 0.12‰.

4.2. Batch HCl alteration experiments

4.2.1. Fluid chemistry

Measurements of dissolved cation concentrations by ICP-OES of fluid samples from B-HCl experiments are given in Table S3. In all experiments, dissolution of basaltic glass was non-stoichiometric. The ratios of Si/Al, Si/Fe, and Si/Mg were low in experimental fluids relative to basalt

glass, suggesting incongruent dissolution or retention of Si in a secondary phase (Fig. 2a and d). The evolution of fluid chemistry over the course of the experiment varied with experimental fluid–rock ratio. In Experiment B-HCl.A, with F/R = 2, concentrations of dissolved phases rose sharply for most elements within the first 24 h of reaction. This period of net dissolution was followed by a drop in all element concentrations by the next sampling session (at 165 h), likely the result of the precipitation of a secondary phase due to reaching high degrees of supersaturation. Dissolved Si concentration ([Si]) dropped from 28 to 1.1 mM while other element concentrations dropped less dramatically, indicating the precipitation of a Si-rich secondary phase. Experiment B-HCl.D, a closed batch experiment lasting 72 h with F/R = 0.3, also demonstrated low Si/Al and Si/Fe ratios but, unlike Experiment B-HCl.A, remained at [Si] above amorphous silica saturation.

Experiment B-HCl.B (F/R = 10) was characterized by a monotonic increase in concentrations of dissolved phases for the first 165 h of reaction and relatively constant concentrations for the remainder of the experiment (Fig. 2b and e). Si/Al and Si/Fe ratios were volatile in early collected samples due to low concentrations but stabilized to values of ~2.5 and ~2.1, respectively, over the course of the experiment. The unchanging concentrations of dissolved solids in the last half of experiment B-HCl.B suggest either that dissolution was passivated by secondary leaching layers on the surfaces of the basalt grains (Gysi and Stefánsson, 2012) or that kinetic basalt dissolution rates had slowed significantly with increasing Al concentrations (Oelkers and Gislason, 2001). Experiment B-HCl.E, a closed experiment run in otherwise identical conditions to B-HCl.B, did not achieve as high [Si] but had similar elemental ratios (Fig. 2b and e).

In experiment B-HCl.C (F/R = 100), dissolved metal concentrations increased monotonically over the entire course of the experiment; steady-state concentrations were not achieved (Fig. 2c). The Si/Fe ratio stabilized at a value similar to the steady-state value observed in Experiment B-HCl.B (~2.1); in contrast, Si/Al stabilized at a lower value (~1.2), corresponding to increased Al mobility and decreased partitioning of Al into secondary phases (Fig. 2c and f). Numerous experimental alteration studies demonstrate increased Al mobility during glass dissolution with decreasing pH (Knauss et al., 1989; Gislason and Oelkers, 2003; Hurowitz et al., 2005). The difference in Si/Al between Experiments B-HCl.B and B-HCl.C is likely attributable to a pH effect. Glass dissolution consumes acidity and drives pH up; at higher F/R, a smaller fraction of acidity is consumed and Al mobility remains high.

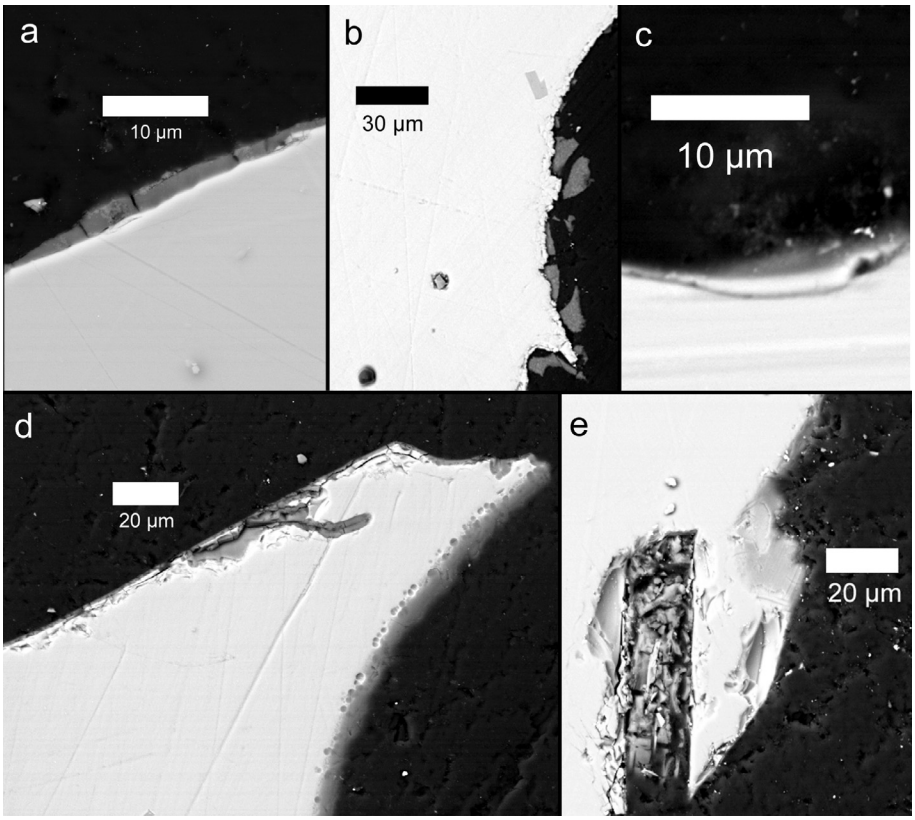

Fig. 3. Alteration product morphologies from batch HCl experiments. (a) Siliceous coating, ~2 μm thick, on a grain collected along with fluid sample B-HCl.A.4. (b) Grain from Experiment B-HCl.A, collected after experiment completion, with a broken layer of Si-rich precipitate 12 μm thick. (c) Experiment B-HCl.B grain. Grains from this experiment showed minimal evidence of alteration products; maximum coating thicknesses observed were 0.5–1 μm. (d) Grain from Experiment B-HCl.C, featuring a 6 μm thick silica alteration layer (on right) and amorphous silica replacing basalt along an interior crack (on left). (e) Replacement of a plagioclase lath by silica in a grain from Experiment B-HCl.C.

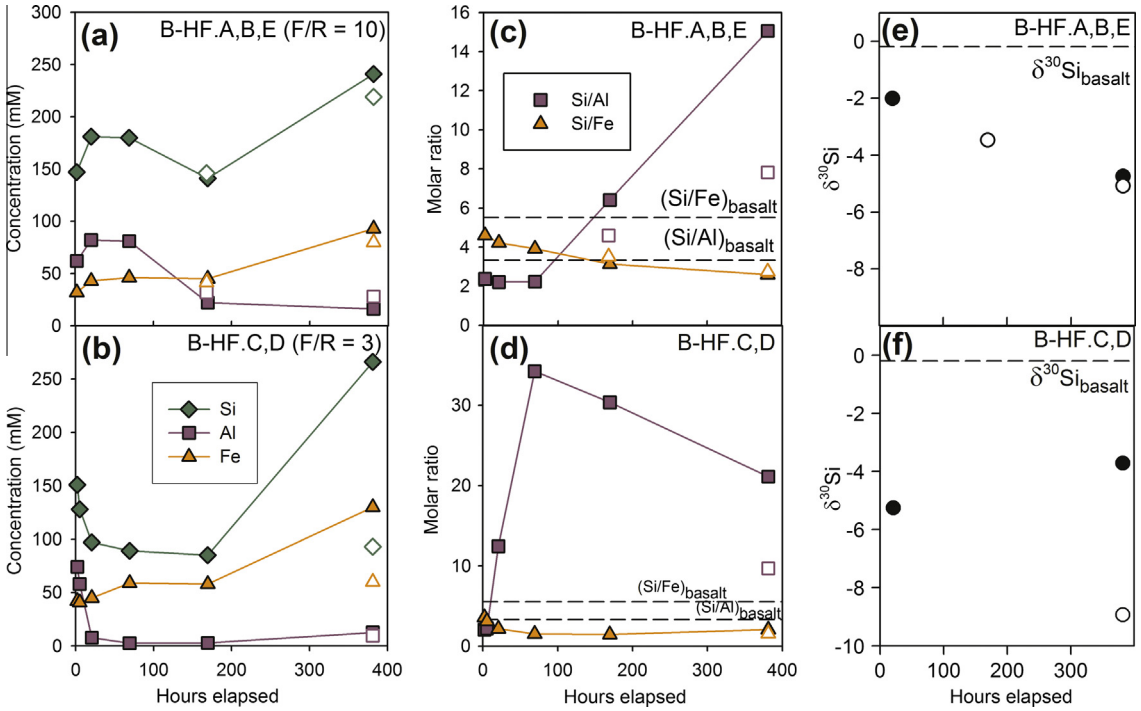

Fig. 4. Elemental concentrations (a and b), elemental molar ratios (c and d), and Si isotope compositions (e and f) of fluids from batch HF alteration experiments. In molar ratio figures (c and d), dotted lines indicate the molar ratio of Si/Fe and Si/Al in KP-fresh basalt. In Si isotope figures (e and f), the dashed line indicates the δ^{30}Si of KP-fresh. (a), (c), and (e) depict experiments B-HF.A (periodic collection, fluid/rock ratio = 10; closed symbols), B-HF.D, and B-HF.E (no collection until conclusion; open symbols). (b), (d), and (f) depict experiments B-HF.C (periodic collection, fluid/rock ratio = 3; closed symbols) and B-HF.D (no collection until conclusion; open symbols).

4.2.2. Alteration phase chemistry and mineralogy

Microimagery of altered basalt grains, collected for the products of experiments B-HCl.A, B-HCl.B, and B-HCl.C, showed evidence of Si-rich leached layers at grain edges (Fig. 3). Boundaries between the alteration layers and the basaltic substrate were sharp at SEM resolution. Basalt grains collected concurrently with B-HCl.A.4 and at the conclusion of experiment B-HCl.A had alteration layers up to 2 μm and 12 μm thick, respectively (Fig. 3a and b). Electron probe microanalysis indicates that these alteration materials are ~75% SiO_2 and ~20% FeO^* (Table S4). Alteration layers on basalt grains from experiment B-HCl.B were present but too thin for microprobe analysis (0.5–1 μm) (Fig. 3c).

Basalt grains from experiment B-HCl.C featured alteration layers up to 6 μm thick (Fig. 6c). The chemistry of the alteration layers from this experiment was heterogeneous. Some layers displayed the Si- and Fe-rich chemistry observed for solids from experiment B-HCl.A; other layers were nearly pure silica (Table S4). In places, acid alteration of the basalt grains penetrated the interiors of grains along cracks (Fig. 3d). Near-surface plagioclase laths were occasionally replaced by silica (Fig. 3e).

4.2.3. Silicon isotope composition of fluids and altered substrate

Fluids from all HCl alteration experiments were enriched in ^{30}Si relative to KP-fresh basalt (Fig. 2g–i; Table 4). The magnitude of Si isotope fractionation varied inversely with F/R. Experiments with low F/R (B-HCl.A and B-HCl.D) achieved δ^{30}Si values of 1.73 ± 0.07‰ and 2.29 ± 0.12‰ (2 s.d.), respectively. Final fluid samples from experiments with high F/R (B-HCl.B, B-HCl.C and B-HCl.E) were 0.90 ± 0.05‰, -0.04 ± 0.15‰, and 1.50 ± 0.51‰, respectively. Fluid δ^{30}Si increased over time in experiments with periodic collection; fluid samples collected early in the course of experiments B-HCl.B and B-HCl.C displayed no isotope fractionation relative to unaltered basalt. These measurements suggest that, contrary to observations by Ziegler et al. (2005), initial basalt dissolution produces no Si isotope fractionation. More intense leaching and/or secondary mineral precipitation may be required for a resolvable isotopic fractionation.

In one experiment, B-HCl.E, bulk altered basalt grains were digested and analyzed for Si isotope composition. The measured value for the bulk solid, $\delta^{30}\text{Si} = -0.23 \pm 0.42$‰, is indistinguishable from unaltered KP-fresh basalt, consistent with the minimal mass of alteration products as documented by SEM.

4.3. Batch HF alteration experiments

4.3.1. Fluid chemistry

Dissolved Si concentrations ([Si]) in HF alteration experiments were considerably higher than those in HCl experiments (Table S5). Final [Si] for experiments conducted with 1 M HF ranged from 93 to 266 mM. Si/Fe

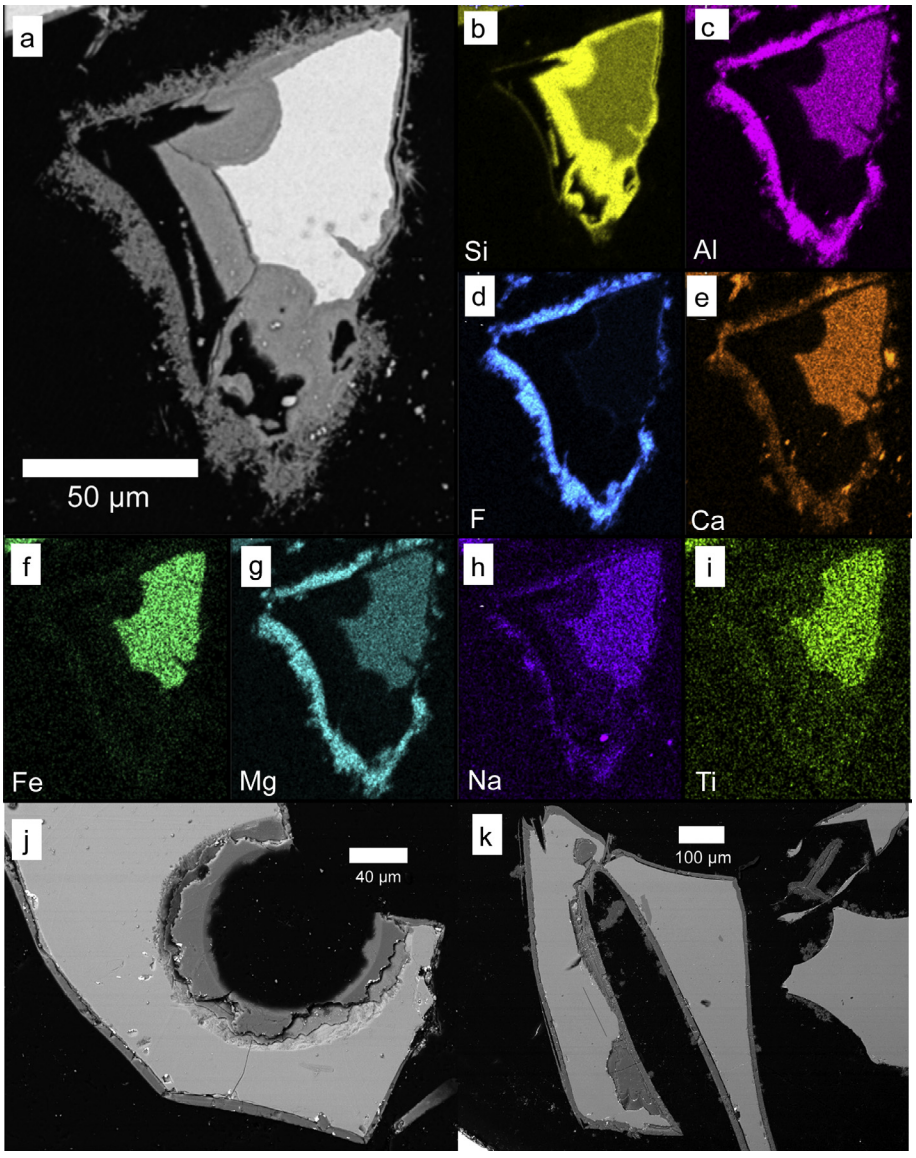

Fig. 5. Alteration product morphologies from batch HF experiments. (a) Grain from Experiment B-HF.A, featuring 30 μm thick amorphous silica layers, formed by dissolution–reprecipitation, and acicular fluoride crystals. (b–i) Elemental maps by EDS of the grain from (a), illustrating that the fluoride deposit contains Ca, Al, Mg, Na, and Fe, but not Si. (j) Grains from Experiment B-HF.B, with Si-rich alteration layers up to 100 μm thick. (k) Grain from Experiment B-HF.C with 5 and 30 μm Si-rich alteration layers.

ratios of experimental fluids started at values close to the Si/Fe ratio of basalt and decreased steadily to ~2.5 over the course of the experiments. Initial Si/Al ratios were also close to basaltic compositions, but rose over the course of the experiments to values much higher than Si/Al ratios in basalt (Fig. 4). Al and Mg concentrations of collected fluids dropped as [Si] remained constant or rose, consistent with the precipitation of an Al-rich, Mg-rich, and Si-poor secondary phase. This observed relative element mobility, nearly reversed from that observed in the batch HCl experiments, is facilitated by high solubility of silicon hexafluoride complexes and insolubility of Al- and Mg-fluorides.

Experiments B-HF.F and B-HF.G were performed with a lower concentration of HF (0.1 M). Final Si concentrations in these experiments were 7.5 to 11.5 mM, respectively. Unlike fluid samples from the other HF experiments, the fluid sample from Experiment B-HF.F had values of Si/Fe and Si/Al ratios lower than basalt stoichiometric ratios. The enhanced Si mobility observed in experiments B-HF.A through D apparently depends on high concentrations of HF for effective Si complexation.

4.3.2. Alteration phase chemistry and mineralogy

Analysis by SEM and EDS of reacted basalt grains from all B-HF experiments revealed extensive alteration of the near-edge basalt and newly formed crystalline precipitates. Basalt grains from experiment B-HF.A were bounded by alteration layers up to 30 μm thick (Fig. 5a). Chemical

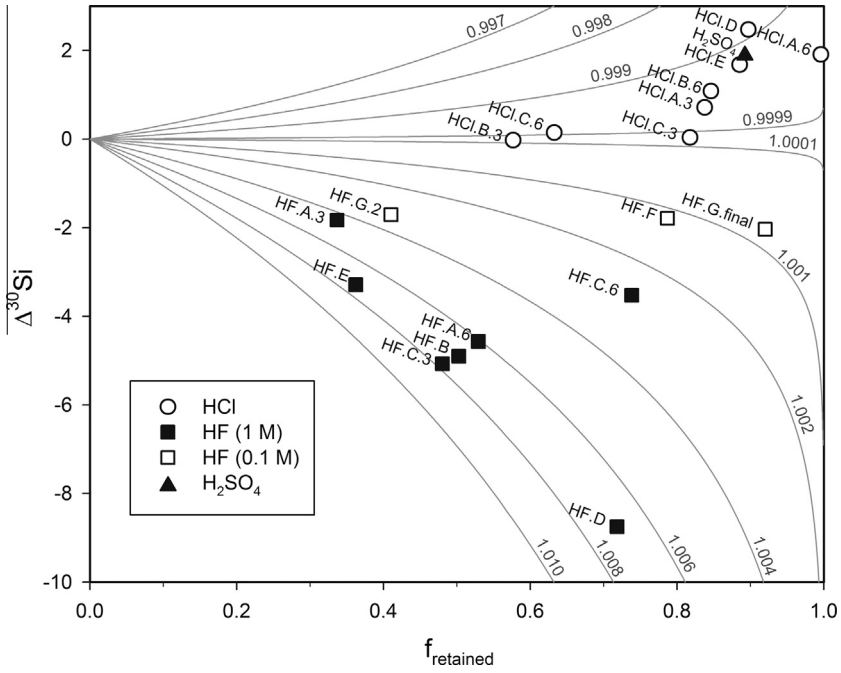

Fig. 6. Calculation of silicon isotope fractionation factors from fluids collected from HCl, HF, and H_2SO_4 batch alteration experiments. See text for methods for determining $f_{retained}$. Gray curves illustrate $\Delta^{30}Si$–$f_{retained}$ trends for specific values of $\alpha_{precip\text{-}Si(aq)}$.

Table 4
MC-ICP-MS silicon isotope analyses of fluids and solids from batch alteration experiments.

Sample	Collection time	Lab	$\delta^{29}Si$	2 s.d.	2 s.e.[a]	$\delta^{30}Si$	2 s.d.	2 s.e.	n[b]
HCl batch experiments									
B-HCl.A.3	23	UCLA	0.34	0.05	0.02	0.53	0.12	0.05	6
B-HCl.A.6	693	UCLA	0.88	0.07	0.03	1.73	0.07	0.03	5
B-HCl.B.3	23	UCLA	−0.09	0.05	0.02	−0.21	0.10	0.04	6
B-HCl.B.6	694	UCLA	0.50	0.02	0.01	0.90	0.05	0.02	6
B-HCl.C.3	23	UCLA	−0.08	0.05	0.02	−0.15	0.05	0.02	6
B-HCl.C.6	694	UCLA	0.00	0.02	0.01	−0.04	0.15	0.06	6
B-HCl.D.final	72	UCLA	1.15	0.12	0.06	2.29	0.12	0.06	4
B-HCl.E.final	165	WU	0.76	0.27	0.12	1.50	0.51	0.23	5
B-HCl.E (final solid)	165	WU	−0.13	0.27	0.12	−0.23	0.42	0.19	5
HF batch experiments									
B-HF.A.3	21	UCLA	−1.09	0.35	0.11	−2.01	0.60	0.19	10
B-HF.A.6	381	UCLA	−2.44	0.12	0.05	−4.75	0.12	0.05	6
B-HF.B.final	381	UCLA	−2.59	0.41	0.13	−5.08	0.70	0.22	10
B-HF.C.3	21	UCLA	−2.71	0.12	0.04	−5.25	0.15	0.05	9
B-HF.C.6	381	UCLA	−1.92	0.02	0.01	−3.71	0.04	0.02	5
B-HF.D.final	381	UCLA	−4.57	0.18	0.06	−8.93	0.21	0.07	9
B-HF.E.final	168	UCLA	−1.76	0.18	0.09	−3.47	0.24	0.12	4
B-HF.F.final	168	UCLA	−1.07	0.28	0.16	−1.97	0.24	0.14	3
B-HF.G.2	72	WU	−0.97	0.18	0.08	−1.89	0.34	0.15	5
B-HF.G.final	168	WU	−1.16	0.13	0.04	−2.22	0.19	0.06	10
B-HF.G (final solid)	168	WU	0.06	0.22	0.07	0.11	0.28	0.09	10
H_2SO_4 batch experiment									
B-H_2SO_4.A.final	168	WU	0.91	0.13	0.06	1.71	0.32	0.13	6
B-H_2SO_4.A (final solid)	168	WU	−0.18	0.10	0.04	−0.35	0.27	0.11	6

[a] Standard error.
[b] Number of analyses.

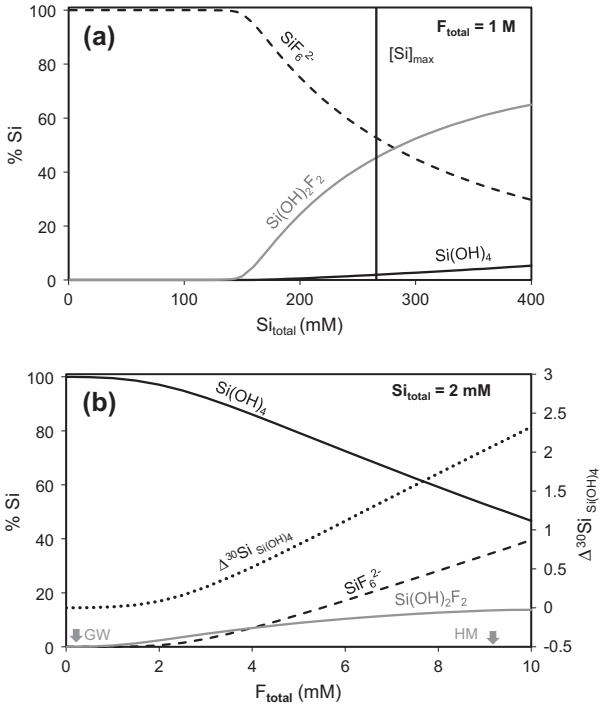

Fig. 7. Models of aqueous Si speciation in the presence of fluorine. Dissolved metals other than Si are ignored and speciation is limited to the three species displayed ($Si(OH)_4$, $Si(OH)_2F_2$, and SiF_6^{2-}). Equilibrium constants for $Si(OH)_2F_2$ and SiF_6^{2-} association are from Busey et al. (1980) and Golovnev et al. (2003). (a) Silica speciation as a function of total dissolved Si at fixed $F_{total} = 1$ M. The vertical line indicates the maximum Si concentration measured in HF batch alteration experiments. (b) Si speciation at low F concentrations at fixed $Si_{total} = 2$ mM. The dotted curve represents the $\Delta^{30}Si$ of aqueous $Si(OH)_4$ relative to total dissolved Si, assuming a fractionation factor of 1000 ln $\alpha_{SiF_6-Si(OH)_4} = +5‰$ and 1000 ln $\alpha_{SiF_6-Si(OH)_4} = +2.5‰$. Gray arrows indicate maximum F concentrations measured in Kilauean groundwater (GW) and in a fumarole at Halemaumau Crater, Kilauea Caldera (HM), from Hurwitz et al. (2003).

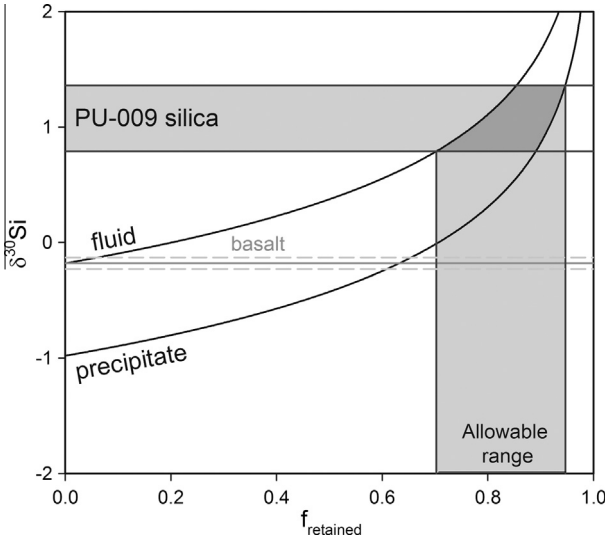

Fig. 8. Rayleigh fractionation modeling of Hawaiian silica coatings, using 1000 ln $\alpha_{precip-Si(aq)} = -0.8‰$. The range of silica coating $\delta^{30}Si$ is illustrated by the gray box; the composition of KP-fresh basalt is given by the solid gray line. Values of $f_{retained}$ between 0.70 and 0.94 are consistent with the composition of the PU-009 silica coating.

Table 5
Calculated values of $f_{retained}$ and $\alpha_{precip-Si(aq)}$ for each experimental fluid analyzed for $\delta^{30}Si$. See text for calculation details.

Sample	$f_{retained,min}$	1000 ln $\alpha_{precip-Si(aq)}$
B-HCl.A.3	0.838	-0.39 ± 0.04
B-HCl.A.6	0.996	-0.34 ± 0.01
B-HCl.B.3	0.577	0.03 ± 0.07
B-HCl.B.6	0.846	-0.57 ± 0.03
B-HCl.C.3	0.818	-0.02 ± 0.04
B-HCl.C.6	0.633	-0.15 ± 0.08
B-HCl.D.final	0.897	-1.09 ± 0.03
B-HCl.E.final	0.886	-0.78 ± 0.11
B-HF.A.3	0.337	4.44 ± 0.48
B-HF.A.6	0.529	6.04 ± 0.09
B-HF.B.final	0.503	6.98 ± 0.32
B-HF.C.3	0.608	7.72 ± 0.11
B-HF.C.6	0.628	2.63 ± 0.04
B-HF.D.final	0.718	6.88 ± 0.07
B-HF.E.final	0.362	7.28 ± 0.29
B-HF.F.final	0.787	1.15 ± 0.10
B-HF.G.2	0.410	3.23 ± 0.30
B-HF.G.final	0.920	0.80 ± 0.03
$B.H_2SO_4$.final	0.893	-0.85 ± 0.06

analysis by EPMA indicates these alteration layers are ~99 wt% SiO_2 (Table S4). Acicular crystals up to 10 μm long were observed on many substrate surfaces. EDS elemental maps indicate that these crystals are Mg-, Al- and Ca- bearing fluorides (Fig. 5b–i). The fluoride domains contain no more than 10 wt% SiO_2 (Fig. 8b; Table S4). Solid products from Experiments B-HF.B, B-HF.C, and B-HF.D displayed similar textures, but varied in the thickness of alteration layers. In Experiment B-HF.B, Si-rich leached layers were up to 100 μm thick (Fig. 5j).

4.3.3. Silicon isotope composition of fluids and altered substrate

In contrast to the batch HCl experiments, analyzed fluids from the batch HF experiments had negative $\delta^{30}Si$ values (Fig. 4e and f; Table 4). Final $\delta^{30}Si$ values of the fluids from 1 M HF experiments ranged from −8.93‰ to −3.47‰; final $\delta^{30}Si$ of the fluids from 0.1 M HF experiments ranged from −2.22‰ to −1.89‰. Experiments with periodic sample collection showed variable isotopic evolution with time. In experiment B-HF.A (F/R = 10), the fluids became isotopically lighter over the course of the experiment; in experiment B-HF.C (F/R = 3), the reverse trend was observed.

Altered basalt grains from Experiment B-HF.G were digested and analyzed for Si isotope composition. The altered solids from this experiment had a $\delta^{30}Si$ value of $0.11 \pm 0.28‰$ (2 s.d.), significantly higher than that of unaltered basalt ($\delta^{30}Si = -0.18‰$). This direction of fractionation is consistent with the strong negative $\delta^{30}Si$ observed in the experimental fluids. We estimate $\delta^{30}Si$ of the Si-rich

alteration product by isotope mass balance, based on the following equation:

$$\delta^{30}Si_{basalt}(f_{unreacted}) + \delta^{30}Si_{fluid}(f_{fluid}) + \delta^{30}Si_{silica}(f_{silica}) = \delta^{30}Si_{basalt} \quad (1)$$

where $f_{unreacted}$, f_{fluid}, and f_{silica} are the fractions of Si in unreacted basalt, fluid, and precipitated silica, respectively. Using the δ^{30}Si values determined for the B-HF.G fluid and solids and estimating $f_{solution}$ and f_{silica} from the calculated minimum value of $f_{retained}$ (see Section 5.1, Table 5), we calculated a δ^{30}Si value of $+1.66 \pm 0.63‰$ (2 s.d., propagated error) for the siliceous solid precipitated in this experiment.

4.4. Batch H_2SO_4 alteration experiment

A single batch alteration experiment was performed in 0.1 M H_2SO_4 with F/R = 10. Concentration measurements by ICP-OES of the final collected solution showed similar dissolved metal ratios (Si/Al, Si/Fe, and Si/Mg) to HCl batch experiments conducted at the same fluid–rock ratio (Table S3). These elemental ratios suggest that secondary phases formed by H_2SO_4 alteration of basalt are Si-rich relative to the basalt substrate. Silicon isotope analysis on experimental fluid and reacted basalt grains revealed δ^{30}Si values of $1.71 \pm 0.32‰$ and $-0.35 \pm 0.27‰$ (2 s.d.), respectively.

5. DISCUSSION

5.1. Experimental Si isotope fractionation factors

5.1.1. Batch HCl experiments

We employ a Rayleigh distillation model to interpret the observed Si isotope fractionations associated with basalt alteration in HCl. An aliquot of the basalt substrate undergoes dissolution; then, a fraction of the aqueous Si mobilized by dissolution ($f_{retained}$) either precipitates from solution or is retained in a leached phase. Purely congruent dissolution, with no precipitation of secondary phases, corresponds to $f_{retained} = 0$; purely incongruent dissolution, in which all Si released from basalt is retained in secondary phases, corresponds to $f_{retained} = 1$. The Si isotope fractionation factor $\alpha_{precip\text{-}Si(aq)}$ for basalt weathering can be determined from $f_{retained}$ by inverting the Rayleigh fractionation equation:

$$R/R_0 = (1 - f_{retained})^{\alpha - 1} \quad (2)$$

where R is the $^{30}Si/^{28}Si$ ratio of aqueous Si in the fluid sample and R_0 is the $^{30}Si/^{28}Si$ ratio of the unaltered basalt.

To estimate $f_{retained}$, we use solution elemental concentrations (Tables S3 and S5) to calculate the mass of reacted basalt ($m_{reacted}$). Given that most major elements of basalt including Al, Mg, Fe, and Ca, but except for Si, are present in low concentrations in precipitated silica, a minimum $m_{reacted}$ for each element is given by the mass of basalt that contains the quantity of that element in solution:

$$m_{reacted,i} = X_{i,soln} \cdot V \cdot (mw)_i / X_{i,bas} \quad (3)$$

where $X_{i,soln}$ is the concentration in moles/liter of the element i in solution, V is the fluid volume, (mw) is the molar weight of the element i, and $X_{i,bas}$ is the mass abundance of the element i in basalt. The minimum $m_{reacted,min}$ is then given by the maximum of the $m_{reacted,i}$. The fraction of retained Si is given by:

$$f_{retained} = V \cdot X_{Si,soln} / m_{reacted,min} / X_{Si,bas} \cdot (mw)_{Si} \quad (4)$$

Because this method generates a minimum bound on $f_{retained}$, the $\alpha_{precip\text{-}Si(aq)}$ values calculated in Eq. (2) represents upper bounds on the magnitude of fractionation. Table S6 provides the full steps taken for calculating α for each experimental fluid. This simple modeling approach includes only one fractionation step and therefore may convolute the effects of two or more individual fractionating processes. However, it provides a framework for exploring the impact of experimental parameters on the bulk fractionation signature of chemical weathering.

The measured Si isotope fractionations and modeled $f_{retained}$ for all batch experiments are illustrated in Fig. 6 and listed in Table 5. Modeled fractionation factors for fluids from HCl batch experiments ranged from 1000 $\ln \alpha_{precip\text{-}Si(aq)} = +0.03 \pm 0.07‰$ to $-1.09 \pm 0.03‰$. These fractionation factors are in the same direction but somewhat smaller than those reported by various authors for opal or clay precipitation (1000 $\ln \alpha_{precip\text{-}Si(aq)} = -1.2‰$ to $-1.5‰$) (Milligan et al., 2004; Geilert et al., 2014).

Modeled fractionation factors varied with experimental conditions, especially with fluid–rock ratio (F/R). The largest modeled 1000 $\ln \alpha_{precip\text{-}Si(aq)}$ were observed in the experiment with the lowest fluid–rock ratio (B-HCl.D; F/R = 0.3); isotope fractionations were smallest in the experiment with the highest fluid–rock ratio (B-HCl.C; F/R = 100). In some experiments with periodic fluid sample collection, δ^{30}Si and the calculated $\alpha_{precip\text{-}Si(aq)}$ changed over the course of the experiment (Figs. 2h, i and 6). Experiments B-HCl.B and B-HCl.C each featured intermediate fluid samples with zero isotope fractionation and final fluid samples with nonzero values of 1000 $\ln \alpha_{precip\text{-}Si(aq)}$. The intermediately sampled fluid in Experiment B-HCl.C is undersaturated with respect to Si, implying that secondary solid formation at that time step was limited to *in situ* leaching rather than precipitation from solution.

The observed variations in $\alpha_{precip\text{-}Si(aq)}$ and the reduced magnitude of the α relative to previous studies suggest that at least two alteration processes, each with a distinct isotope signature, operated during the HCl batch alteration experiments: (1) *in situ* glass dissolution coupled with formation of Si-rich residues (i.e. glass leaching) ($\alpha_{precip\text{-}Si(aq)} \cong 0$), and (2) silica precipitation from solution (1000 $\ln \alpha_{precip\text{-}Si(aq)} \cong -1‰$). The observed isotopic fractionations from these experiments are smaller than those observed in pure precipitation experiments ($-1.2‰$ to $-1.5‰$; Milligan et al., 2004; Geilert et al., 2014) because some silica formation proceeds by direct replacement. The lack of an isotope effect associated with *in situ* silica residue formation suggests that the process of Si removal from the basaltic glass network during alteration is non-selective with respect to isotopic mass.

5.1.2. Batch H_2SO_4 experiment

The fractionation factor α for the single batch H_2SO_4 experiment, using the method described in the previous

section, is $1000\ \ln \alpha_{\text{precip-Si(aq)}} = -0.85 \pm 0.06‰$ (Fig. 6, Table 5). This α falls within the range of fractionation factors observed for alteration by HCl. The similarity in fractionation behavior between HCl and H_2SO_4 dissolution of basalt glass is attributable to similar speciation of Si in solution. Silicon chloride complexes hydrolyze readily in water, and the existence of silicon sulfate complexes is speculative (Marshall and Chen, 1982); thus, in both sets of experiments, Si occurred in solution as silicic acid monomers and oligomers.

5.1.3. Batch HF experiments

In contrast to fluids from the HCl and H_2SO_4 batch experiments, which evolved towards higher $\delta^{30}Si$ values over the course of a given experiment, all fluid samples from the batch HF experiments were ^{30}Si-depleted relative to the basalt substrate. Derived final fractionation factors ($1000\ \ln \alpha_{\text{precip-Si(aq)}}$) ranged between 0.80‰ and 1.15‰ for experiments in 0.1 M HF and between 2.62‰ and 7.72‰ for experiments in 1 M HF (Fig. 6; Table 5).

We first assess if the ^{30}Si-depleted fluid compositions could be attributable to open system behavior (i.e. leaking of Si-bearing vapor). Equilibrium Si isotope fractionation factors between gaseous SiF_4 and aqueous silica, or between gaseous SiF_4 and solid silicates, have not been measured experimentally. A calculation of the equilibrium fractionation factor between gaseous SiF_4 and solid SiO_2, based on isotope-substituted infrared spectra of SiF_4, indicates a fractionation factor $1000\ \ln \alpha_{\text{SiF4-qtz}} = 14.7 \pm 1.9‰$ at 25 °C, with ^{30}Si concentrating in the SiF_4 vapor (Supplemental Information). The magnitudes of the fractionation factors between different silicate phases, and between solid and aqueous silica, are small relative to $\alpha_{\text{SiF4-qtz}}$ (Meheut et al., 2009). Thus, escaped SiF_4 gas would drive the residual fluid towards lower $\delta^{30}Si$. However, open-system behavior cannot entirely explain the negative $\delta^{30}Si$, as mass losses from the experiments were minimal. Experiments B-HF.E and B-HF.F were weighed before and after reaction and lost only 2.5 and 2.9 mg, respectively. Vapors in equilibrium with dilute H_2SiF_6 solutions are ~10× depleted in Si relative to the solution (Munter et al., 1947), so maximum Si loss fractions ($V_{\text{lost}}/V_{\text{total}}/10$) are 0.12% and 0.14%, respectively. In contrast, achieving the fluid Si isotope compositions ($\delta^{30}Si_{\text{B-HF.E.final}} = -3.47‰$; $\delta^{30}Si_{\text{B-HF.F.final}} = -1.97‰$) by Rayleigh fractionation of SiF_4 gas with $1000\ \ln \alpha = 14.7‰$ would require 20% and 12% of dissolved Si to be lost from the system, respectively. The maximum losses of SiF_4 vapor are too small to explain the observed fractionations, so we dismiss the hypothesis that the HF batch experiments are dominated by open-system behavior.

A second possible cause of the observed ^{30}Si-depleted fluid compositions is Si isotope fractionation between multiple coexisting Si-bearing aqueous species. Many members of the family of Si-hydroxyfluoride complexes $[SiF_x(OH)_y^{4-x-y}]$ are theoretically possible, but the dominant species at high F concentrations are SiF_6^{2-} (hexafluorosilicate) and $Si(OH)_2F_2$ (Busey et al., 1980). At 25 °C, the association reaction for hexafluorosilicate,

$$Si(OH)_4 + 4H^+ + 6F^- \leftrightarrow SiF_6^{2-} + 4H_2O \quad (5)$$

has a measured equilibrium constant of $10^{29.5}$ (Busey et al., 1980; Golovnev et al., 2003). The analogous association reaction for $Si(OH)_2F_2$ has a calculated equilibrium constant of $10^{11.09}$ (Busey et al., 1980). For systems in which $F/Si < 6$, aqueous silicic acid $[Si(OH)_{4(aq)}]$ may co-occur in non-negligible concentrations with these Si-hydroxyfluoride species. We calculate the expected Si speciation given total concentrations of Si and F, ignoring other dissolved cations and using Eq. (5), association reactions for $Si(OH)_2F_2$ and HF, charge balance, and mass balance equations for Si and F. At 1 M HF, SiF_6^{2-} is the dominant Si-bearing species up to concentrations of ~280 mM Si. $Si(OH)_2F_2$ occurs as ~1% of dissolved Si at $[Si] > 150$ mM and surpasses SiF_6^{2-} at 280 mM Si (Fig. 7a). Many of our HF batch experiments achieved [Si] corresponding to non-negligible $Si(OH)_2F_2$, suggesting that the experiments reached conditions in which multiple Si-bearing aqueous species coexisted. Co-existing Si-bearing aqueous species may also occur in Si-saturated solutions with F concentrations as low as 2 mM (Fig. 7b).

Energy dispersive X-ray maps of altered grains from the HF experiments indicate that Si is not a major component of precipitated fluoride minerals (Fig. 5b and d). Si-bearing precipitates likely formed from aqueous silicic acid and not from Si-hydroxyfluoride complexes. Thus, the observed bulk isotopic fractionations could be imparted by fractionations between aqueous species and preferential removal of $Si(OH)_{4(aq)}$ from solution. A first-principles calculation of the fractionation factor between silicic acid and F-bearing aqueous silica species ($\alpha_{SiF_6(aq)-SiO_2(aq)}$) is beyond the scope of this paper. The octahedral coordination of Si in SiF_6^{2-} would favor the lighter isotopes relative to the tetrahedrally coordinated $Si(OH)_4$, all else equal, but differences in charge distribution in Si–F and Si–OH bonds may also affect the fractionation factor. A rough estimate of $\alpha_{SiF_6(aq)-SiO_2(aq)}$ may be derived from experiment B-HF.G, for which $\delta^{30}Si$ was determined for both liquid and solid products. The calculated $\delta^{30}Si$ of the siliceous precipitate from that experiment ($+1.66 \pm 0.63‰$; see Section 4.3.3) implies that aqueous $Si(OH)_4$ was isotopically heavier ($\delta^{30}Si \cong +2.8‰$, assuming $\alpha_{\text{amSi-SiO}_2(aq)} \cong -1.2$ from Geilert et al. (2014)). Thus, the fractionation between $SiF_{6(aq)}^{2-}$ ($-2.22‰$; Table 4) and $Si(OH)_{4(aq)}$ is approximately +5‰. These results imply that Si speciation may have drastic effects on the isotopic signature of chemical weathering in high-fluorine environments.

5.2. Origin of Hawaiian silica coatings and cements

All of the Hawaiian silica coatings and cements analyzed in this study are ^{30}Si-enriched relative to their basaltic substrates. This direction of fractionation is unusual and apparently contradicts previous studies showing that Hawaiian soils become increasingly ^{30}Si-depleted with age (Ziegler et al., 2005; Bern et al., 2010) and that Hawaiian groundwater and stream waters are ^{30}Si-enriched (Georg et al., 2007). Here we consider two potential formation processes that could produce silica coatings with high $\delta^{30}Si$

values: (1) *in situ* derivation of silica by an alteration process with a Si isotope fractionation factor $\alpha_{precip\text{-}Si(aq)} > 1$, and (2) Delivery of ^{30}Si-enriched fluids to sites of silica accumulation.

5.2.1. In situ coating formation

Previously reported field and microtextural characterization of Hawaiian silica coatings was consistent with an *in situ* formation mechanism involving coupled dissolution of surficial basalt by environmentally-derived acids and reprecipitation of a Si-rich layer (Chemtob et al., 2010; Chemtob and Rossman, 2014). However, formation of high-δ^{30}Si silica coatings by an *in situ* leaching process is inconsistent with previously reported Si isotope fractionation factors for opal precipitation ($1000 \ln \alpha_{precip\text{-}Si(aq)} = -1.2‰$ to $-1.5‰$). An *in situ* formation mechanism, if it is the dominant formation process for Hawaiian silica coatings, must operate with a net fractionation factor greater than 1. A solid precipitate forming in equilibrium with a solution has an isotope composition $R_{precip} = \alpha R_{solution}$; when converted to δ notation, this relationship is well approximated by $\delta^{30}Si_{precip} = \delta^{30}Si_{solution} + 1000 \ln \alpha$. This equation implies that *in situ* production of a precipitate with the composition of the most ^{30}Si-enriched coating (PU-009, $\delta^{30}Si = +1.36‰$) from a solution with the composition of basalt ($\delta^{30}Si = -0.18‰$) requires that $1000 \ln \alpha_{precip\text{-}Si(aq)}$ be larger than $\delta^{30}Si_{PU\text{-}009} - \delta^{30}Si_{basalt}$, or larger than $+1.54‰$. Effective $1000 \ln \alpha_{precip\text{-}Si(aq)}$ that are positive but smaller than $+1.54‰$ can produce precipitates with high δ^{30}Si values by Rayleigh fractionation, but only if precipitates are constantly removed from the system (i.e., non-*in situ* formation).

We first consider the role of aqueous Si speciation in modifying the effective $\alpha_{precip\text{-}Si(aq)}$ during chemical weathering. As discussed in Section 5.1.3, complexation of Si in Si-hydroxyfluoride complexes may lead to the precipitation of ^{30}Si-enriched secondary solids. Hydrofluoric acid is a small but significant component of gases emitted from Kilauea. Typical emitted gases associated with Kilauean eruptions in 1983–1984 were 0.20% and 0.25% HF for the ERZ plume and summit plumes, respectively (Greenland et al., 1985; Gerlach, 1993). At the H_2O-rich end of the H_2O-HF system, the liquid phase in equilibrium with vapor is highly enriched in HF relative to the vapor (Munter et al., 1947); therefore, liquid water present on basalt surfaces would scour HF from volcanic fumes. However, HF does not remain in the surficial environment for extended periods after eruption ceases. White and Hochella (1992) repeatedly measured F and Si concentrations by X-ray photoelectron spectroscopy on the surface of a 1987 Kilauea flow after emplacement; they observed the disappearance of surficial F after 270 days. However, textural evidence suggests that silica coatings continue to develop for years after lava emplacement (Chemtob and Rossman, 2014). Therefore, Si-fluoride complexation is unlikely to strongly affect the direction and magnitude of Si isotope fractionation during surficial Hawaiian basalt weathering, although it may cause a measurable fractionation in fumarolic environments with higher F concentrations (Fig. 7b).

A second process that could potentially induce a positive effective Si isotope fractionation factor is Si release from the glass matrix during incongruent dissolution. Ziegler et al. (2005) observed that in low-degree basalt dissolution experiments, leachates had δ^{30}Si up to $3‰$ lower than the substrate basalt. This trend reversed itself at higher degrees of dissolution and was more pronounced for crystalline basalts than for glassy basalts. However, this apparent positive isotope fractionation factor was not replicated in experiments presented in this study; leachates undersaturated with respect to amorphous silica were isotopically unfractionated (Table 4). Therefore, although *in situ* alteration of surficial basalt is observed to occur at Kilauea (Chemtob et al., 2010; Chemtob and Rossman, 2014), it is unlikely to be the volumetrically dominant process of silica coating formation.

5.2.2. Deposition of transported silica

The Si isotope compositions of Hawaiian siliceous alteration materials instead support a formation mechanism involving transport and deposition of ^{30}Si-enriched silica at the basalt surface. Applying a Si isotope fractionation factor consistent with the HCl and H_2SO_4 alteration experiments presented in this study ($1000 \ln \alpha_{precip\text{-}aqueous} = -0.8‰$), we model the isotopic evolution of solutions interacting with basalt by Rayleigh fractionation (Fig. 8). Initial precipitates from the dissolving solution are ^{30}Si-depleted relative to the basalt substrate, but ^{30}Si-enriched compositions may be achieved by isolation or removal of the secondary precipitates from the altering fluid. To achieve the δ^{30}Si range observed for Hawaiian silica coatings and cements ($0.79–1.37‰$), the majority ($f_{retained} = 0.70–0.95$) of Si mobilized by acidic dissolution must be retained in leached or secondary phases, presumably in the near-subsurface. That evolved fluid is then transported to the basalt surface, where it evaporates and evaporatively deposited at the basalt surface.

The silica-indurated soil sample S-12-41 provides a unique constraint on the silica coating formation mechanism. Like the coatings, the Si-rich cement from S-12-41 was ^{30}Si-enriched (Table 3). Deposition of a silica cement requires the transport and evaporation of silica-bearing solution (Flach et al., 1969; Seelos et al., 2010), so its isotopic signature reflects a Rayleigh process. The similarity in δ^{30}Si between the cement and surface coatings suggest that they share a formation mechanism. If *in situ* leaching dominated formation of surface coatings, such that ^{30}Si-enriched silica was retained in coatings and ^{30}Si-depleted silica was mobilized in solution, then subsurface depositional cements might have the isotopic composition of the mobilized Si (^{30}Si-depleted). Instead, the observation that the coatings and siliceous cements are both ^{30}Si-enriched suggests that both are dominated by transport and emplacement of subsurface-derived silica.

A potential weakness of the formation model involving Rayleigh fractionation and deposition is the scarcity of ^{30}Si-depleted reservoirs observed in the near-surface environment. The only sample collected that was isotopically lighter than KP-fresh was the interior of the 1974 Ka'u Desert basalt KD-005 ($\delta^{30}Si = -0.84‰$). Sample KD-005 was structurally coherent but has apparently undergone substantial chemical weathering, although contiguous

pockets of ^{30}Si-depleted secondary minerals were not obviously present in SEM images. The ^{30}Si-depleted secondary mineral deposits may be distributed diffusely throughout a relatively large mass of interior basalt, rather than occurring as massive opal precipitation. Alternately, our sampling campaign may have missed these reservoirs entirely. All samples described in this study were collected within a few centimeters of the subaerial flow surface; perhaps the isotopically light minerals are concentrated in a lower horizon within the flows.

Although silicon isotopes indicate that silica coating formation was primarily depositional, morphological evidence suggests that *in situ* surficial alteration occurred at least locally. Siliceous alteration layers were observed to bridge near-surface vesicles and etch surficial nubs in a manner implying replacement (Chemtob et al., 2010; Chemtob and Rossman, 2014). Both residual and depositional processes likely operate; some coatings feature multiple distinct layers, implying repeated leaching and silica deposition (Chemtob and Rossman, 2014). The Rayleigh fractionation model predicts that residual and depositional coating layers should have different δ^{30}Si values. Silica produced by *in situ* leaching should be unfractionated or isotopically light; silica emplaced by fluid transport and evaporation should be isotopically heavy. A high spatial resolution isotope measurement (e.g. SIMS) to attempt to resolve isotopic differences between alteration morphologies has not been pursued in this work but would serve as a test for the model presented here.

5.3. Implications for weathering environments

The analyses of Hawaiian silica coatings and cements presented here expand the δ^{30}Si range observed globally for secondary minerals in weathering environments. The high δ^{30}Si values of these materials are in apparent conflict with observations that stream waters draining the Hawaiian islands are ^{30}Si-enriched relative to basalt (Georg et al., 2007), suggesting that ^{30}Si-enriched secondary minerals are volumetrically minor and require unusual environmental conditions to form. Environments with low fluid–rock ratio are likely most conducive to the high degrees of Rayleigh fractionation required to precipitate ^{30}Si-enriched silica. Annual rainfall accumulation at the study sites ranges from ~1500 mm at the Kilauea summit to ~3500 mm near Pu'u O'o (Giambelluca et al., 2013), considerably higher than the threshold for desert conditions. However, the high porosity and infiltration capacity of freshly erupted lava flows and tephra inhibits standing water and runoff (Malin et al., 1983), so surficial water–rock interactions occur primarily at low F/R. These conditions are not limited to Hawaii; Rayleigh-dominated secondary mineral precipitation is expected to occur in subaerial weathering environments with similarly high infiltration capacity or with lower rainfall rates. Evaporative Rayleigh fractionation in these low F/R settings has only a minor effect on the macroscopic weathering trend, but should produce observable δ^{30}Si variability in secondary minerals at the local scale.

A prediction of our model of Hawaiian silica coating formation, which involves both *in situ* basalt leaching and deposition of ^{30}Si-enriched silica, is isotopic variability within the silica coatings at the microtextural scale. This fine-scale heterogeneity in δ^{30}Si may be detectable in the geologic record as a paleoclimatic signature of low F/R conditions. This process would be most observable in paleosols or other sequences implying subaerial exposure. Fine-scale variation of δ^{30}Si has already been observed in microanalytical studies of ancient ocean floor sediments (Steinhoefel et al., 2009, 2010; Marin-Carbonne et al., 2011; Stefurak et al., 2015), although those heterogeneities were derived in vastly different conditions from the setting of this study. Our findings suggest that the range of δ^{30}Si values of ancient rocks at the microtextural scale, in addition to their bulk δ^{30}Si, may convey important information about the history of fluid alteration for a variety of depositional environments.

Our experimental results show that the bulk Si isotope fractionation factor for chemical weathering is not constant, but rather varies with fluid–rock ratio and fluid composition. Incongruent dissolution of basalt in silica-undersaturated fluids is apparently associated with a near-zero fractionation factor, while precipitation of secondary minerals from solution has a fractionation factor of 1–1.5‰. In conditions where both processes occur simultaneously, an intermediate fractionation factor may be appropriate; for our HCl and H_2SO_4 experiments, $1000 \ln \alpha = 0.8‰$ fit the Si isotope compositions of the fluids well. Recent studies indicate that Si isotope fractionation factors also depend on temperature and kinetic rate of precipitation (Oelze et al., 2014; Geilert et al., 2015). Thus, interpretation of Si isotopes in modern weathering systems requires a parameterization of α, rather than a single bulk Si isotope fractionation factor. A testable prediction of this experimental finding is that waters that have interacted with different volumes of the same bedrock (i.e. river water and percolated groundwater) will have different δ^{30}Si. Similarly, efforts to reconstruct the δ^{30}Si of precipitating fluids in the geologic record (e.g. de la Rocha et al., 1998; Robert and Chaussidon, 2006) may require additional constraints on the conditions of precipitation to accurately select the appropriate fractionation factor.

Our experiments also have special implications for Si isotope fractionation in fluorine-rich systems. Secondary minerals precipitating in the presence of 0.1 and 1 M HF have heavy Si isotope compositions relative to their substrate. Speciation calculations suggest that silica precipitating from fluids with F concentrations more typical of natural waters may also display large anomalous isotope fractionations (Fig. 7b). At amorphous silica saturation, Si-hydroxyfluorides occur in significant quantities (>10% of Si_{total}) at F_{total} above 3 mM. Assuming a 5‰ δ^{30}Si fractionation between SiF_6^{2-} and $Si(OH)_4$, and a 2.5‰ fractionation between $SiF_2(OH)_2$ and $Si(OH)_4$, we predict a resolvable (0.1‰) fractionation in δ^{30}Si for F concentrations at or above 2 mM (Fig. 7b). Natural waters with $F_{total} \geqslant 2$ mM are uncommon but observable, especially in association with fumaroles, peralkaline volcanic terrains, and rift valleys (Edmunds and Smedley, 2005). At the Kilauea summit,

groundwater was measured to have a maximum F concentration of 0.15 mM, but condensates at Halemaumau Crater contain up to 9.21 mM (Fig. 7b; Hurwitz et al., 2003). F concentration excess of 100 mM have been observed in East African Rift Valley lakes and hot springs (Jones et al., 1977; Nanyaro et al., 1984). Our experimental results suggest that anomalous Si isotope signatures should be observable in these environments. Vapor-deposited silica in F-rich silicic volcanic environments may also display the isotopic signature of Si-fluoride complexation (Naboko, 1957; de Hoog et al., 2005; Horwell et al., 2013).

6. CONCLUSIONS

Amorphous silica coatings and cements on 10- to 40-year old basalts at Kilauea Volcano, Hawai'i, are enriched in heavy Si isotopes ($\delta^{30}Si = +0.80$ to 1.36‰) relative to their basalt substrate. Batch dissolution experiments on fresh basaltic glass indicated that Si isotope fractionation factors are strongly affected by fluid–rock ratio and aqueous speciation. Observed fractionations were near-zero for early time steps in high fluid–rock ratio experiments, implying that Si isotope fractionation is driven by secondary mineral precipitation and not by Si release during glass dissolution. Basalt dissolution in HCl and H_2SO_4 preferentially released isotopically heavy Si into solution; in contrast, basalt dissolution in HF preferentially released isotopically light Si, producing secondary minerals with high $\delta^{30}Si$. The anomalous Si isotope signature in HF experiments is attributed to fractionation between coexisting aqueous silicic acid and Si-hydroxyfluorides. However, the two most common volatile components present in Hawaiian volcanic gases (H_2SO_4 and HCl) are not associated with an atypical fractionation direction. Thus, ^{30}Si-enriched Kilauean silica deposits are likely derived by incongruent dissolution of basalt, releasing $\delta^{30}Si$ into solution, followed by transport and evaporative deposition of the mobilized Si at the basalt surface.

ACKNOWLEDGEMENTS

Financial support was provided to GRR by the White Rose Foundation and by the National Aeronautics and Space Administration – United States (NESSF, NNX09AT77H). We thank Samantha Ingalls (UCLA) and Paul Savage, Emily Pringle, and Julien Foriel (WU) for assistance with MC-ICP-MS data collection and Don Swanson (HVO-USGS) for samples and discussion. We thank Grit Steinhoefel, two anonymous reviewers, and Associate Editor Clark Johnson for input that greatly improved the manuscript.

APPENDIX A. SUPPLEMENTARY DATA

Supplementary data associated with this article can be found, in the online version, at http://dx.doi.org/10.1016/j.gca.2015.07.026.

REFERENCES

Alleman L. Y., Cardinal D., Cocquyt C., Plisnier P.-D., Descy J. P., Kimirei I., Sinyinza D. and André L. (2005) Silicon isotopic fractionation in Lake Tanganyika and its main tributaries. *J. Great Lakes Res.* **31**, 509–519.

Armytage R. M. G., Georg R. B., Savage P. S., Williams H. M. and Halliday A. N. (2011) Silicon isotopes in meteorites and planetary core formation. *Geochim. Cosmochim. Acta* **75**, 3662–3676.

Azaroual M., Fouillac C. and Matray J. M. (1997) Solubility of silica polymorphs in electrolyte solutions. 1. Activity coefficient of aqueous silica from 25 degrees to 250 degrees C, Pitzer's parameterisation. *Chem. Geol.* **140**, 155–165.

Bai S. Q., Urabe S., Okaue Y. and Yokoyama T. (2009) Acceleration effect of sulfate ion on the dissolution of amorphous silica. *J. Colloid Interface Sci.* **331**, 551–554.

Basile-Doelsch I., Meunier J. D. and Parron C. (2005) Another continental pool in the terrestrial silicon cycle. *Nature* **433**, 399–402.

Bern C., Brzezinski M., Beucher C., Ziegler K. and Chadwick O. (2010) Weathering, dust, and biocycling effects on soil silicon isotope ratios. *Geochim. Cosmochim. Acta* **74**, 876–889.

Busey R. H., Schwartz E. and Mesmer R. E. (1980) Fluorosilicate equilibria in sodium-chloride solutions from 0 to 60 °C. *Inorg. Chem.* **19**, 758–761.

Cardinal D., Gaillardet J., Hughes H. J., Opfergelt S. and André L. (2010) Contrasting silicon isotope signatures in rivers from the Congo Basin and the specific behaviour of organic-rich waters. *Geophys. Res. Lett.* **37**, L12403. http://dx.doi.org/10.1029/2010GL043413.

Chakrabarti R., Knoll A. H., Jacobsen S. B. and Fischer W. W. (2012) Si isotope variability in Proterozoic cherts. *Geochim. Cosmochim. Acta* **91**, 187–201.

Chemtob S. M. and Rossman G. R. (2014) Timescales and mechanisms of formation of amorphous silica coatings on fresh basalts at Kilauea Volcano, Hawai'i. *J. Volcanol. Geotherm. Res.* **286**, 41–54.

Chemtob S. M., Jolliff B. L., Rossman G. R., Eiler J. M. and Arvidson R. E. (2010) Silica coatings in the Ka'u Desert, Hawaii, a Mars analog terrain: a micromorphological, spectral, chemical, and isotopic study. *J. Geophys. Res. Planets*. http://dx.doi.org/10.1029/2009JE003473.

Chemtob S. M., Rossman G. R. and Stebbins J. F. (2012) Natural hydrous amorphous silica: quantitation of network speciation and hydroxyl content by ^{29}Si MAS NMR and vibrational spectroscopy. *Am. Mineral.* **97**, 203–211.

Chen C. T. A. and Marshall W. L. (1982) Amorphous silica solubilities. 4. Behavior in pure water and aqueous sodium chloride, sodium sulfate, magnesium chloride, and magnesium sulfate solutions up to 350 °C. *Geochim. Cosmochim. Acta* **46**, 279–287.

Chmeleff J., Horn I., Steinhoefel G. and von Blanckenburg F. (2008) In situ determination of precise stable Si isotope ratios by UV-femtosecond laser ablation high-resolution multi-collector ICP-MS. *Chem. Geol.* **249**, 155–166.

Das A., Krishnaswami S., Sarin M. M. and Pande K. (2005) Chemical weathering in the Krishna Basin and Western Ghats of the Deccan Traps, India: rates of basalt weathering and their controls. *Geochim. Cosmochim. Acta* **69**, 2067–2084.

de Hoog J. C. M., van Bergen M. J. and Jacobs M. H. G. (2005) Vapour-phase crystallisation of silica from SiF4-bearing volcanic gases. *Ann. Geophys.* **48**, 775–785.

de la Rocha C. L., Brzezinski M. A. and DeNiro M. J. (1996) Purification, recovery, and laser-driven fluorination of silicon from dissolved and particulate silica for the measurement of natural stable isotope abundances. *Anal. Chem.* **68**, 3746–3750.

de La Rocha C. L., Brzezinski M. A., DeNiro M. J. and Shemesh A. (1998) Silicon-isotope composition of diatoms as an indicator of past oceanic change. *Nature* **395**, 680–683.

de la Rocha C. L., Brzezinski M. A. and DeNiro M. J. (2000) A first look at the distribution of the stable isotopes of silicon in natural waters. *Geochim. Cosmochim. Acta* **64**, 2467–2477.

Delstanche S., Opfergelt S., Cardinal D., Elsass F., Andre L. and Delvaux B. (2009) Silicon isotopic fractionation during adsorption of aqueous monosilicic acid onto iron oxide. *Geochim. Cosmochim. Acta* **73**, 923–934.

Ding T., Wan D., Wang C. and Zhang F. (2004) Silicon isotope compositions of dissolved silicon and suspended matter in the Yangtze River, China. *Geochim. Cosmochim. Acta* **68**, 205–216.

Douthitt C. B. (1982) The geochemistry of the stable isotopes of silicon. *Geochim. Cosmochim. Acta* **46**, 1449–1458.

Edmunds W. M. and Smedley P. L. (2005) Fluoride in natural waters. In *Essentials of Medical Geology – Impacts of the Natural Environment on Public Health* (eds. O. Selinus, B. Alloway, J. A. Centeno, R. B. Finkelman, R. Fuge, U. Lindh and P. Smedley). Elsevier, pp. 301–315.

Flach K. W., Nettleton W. D., Gile L. H. and Cady J. G. (1969) Pedocementation: induration by silica, carbonates, and sesquioxides in the quaternary. *Soil Sci.* **107**, 442–453.

Fulignati P., Sbrana A., Clocchiatti R. and Luperini W. (2006) Environmental impact of the acid fumarolic plume of a passively degassing volcano (Vulcano Island, Italy). *Env. Geol.* **49**, 1139–1155.

Geilert S., Vroon P. Z., Roerdink D. L., Van Cappellen P. and Van Bergen M. J. (2014) Silicon isotopic fractionation during abiotic silica precipitation at low temperatures: inferences from flow-through experiments. *Geochim. Cosmochim. Acta* **142**, 95–114.

Geilert S., Vroon P. Z., Keller N. S., Gudbrandsson S., Stefansson A. and van Bergen M. J. (2015) Silicon isotope fractionation during silica precipitation from hot-spring waters: evidence from the Geysir geothermal field, Iceland. *Geochim. Cosmochim. Acta* **164**, 403–427.

Georg R. B., Reynolds B. C., Frank M. and Halliday A. N. (2006) Mechanisms controlling the silicon isotopic compositions of river waters. *Earth Planet. Sci. Lett.* **249**, 290–306.

Georg R. B., Reynolds B. C., West A. J., Burton K. W. and Halliday A. N. (2007) Silicon isotope variations accompanying basalt weathering in Iceland. *Earth Planet. Sci. Lett.* **261**, 476–490.

Georg R. B., Zhu C., Reynolds B. C. and Halliday A. N. (2009) Stable silicon isotopes of groundwater, feldspars, and clay coatings in the Navajo sandstone aquifer, Black Mesa, Arizona, USA. *Geochim. Cosmochim. Acta* **73**, 2229–2241.

Gerlach T. M. (1993) Oxygen buffering of Kilauea volcanic gases and the oxygen fugacity of Kilauea basalt. *Geochim. Cosmochim. Acta* **57**, 795–814.

Giambelluca T. W., Chen Q., Frazier A. G., Price J. P., Chen Y.-L., Chu P.-S., Eischeid J. K. and Delparte D. M. (2013) Online rainfall atlas of Hawai'i. *Bull. Am. Meteor. Soc.* **94**, 313–316. http://dx.doi.org/10.1175/BAMS-D-11-00228.1.

Gislason S. R. and Oelkers E. H. (2003) Mechanism, rates and consequences of basaltic glass dissolution: II. An experimental study of the dissolution rates of basaltic glass as a function of pH and temperature. *Geochim. Cosmochim. Acta* **67**, 3817–3832.

Golovnev N. N., Nogteva V. B. and Golovneva I. I. (2003) Formation of Si(IV) and Ge(IV) fluoride complexes in dilute aqueous solutions. *Russ. J. Gen. Chem.* **73**, 1388–1394.

Gordon S. J. and Dorn R. I. (2005) In situ weathering rind erosion. *Geomorphology* **67**, 97–113.

Greenland L. P., Rose W. I. and Stokes J. B. (1985) An estimate of gas emissions and magmatic gas content from Kilauea volcano. *Geochim. Cosmochim. Acta* **49**, 125–129.

Gysi A. P. and Stefánsson A. (2012) Mineralogical aspects of CO_2 sequestration during hydrothermal basalt alteration – an experimental study at 75 to 250 °C and elevated pCO_2. *Chem. Geol.* **306–307**, 146–159.

Heck P. R., Huberty J. M., Kita N. T., Ushikubo T., Kozdon R. and Valley J. W. (2011) SIMS analyses of silicon and oxygen isotope ratios for quartz from Archean and paleoproterozoic banded iron formations. *Geochim. Cosmochim. Acta* **75**, 5879–5891.

Hellmann R., Daval D. and Wirth R. (2013) Formation of amorphous silica surface layers by dissolution–reprecipitation during chemical weathering: implications for CO_2 uptake. *Proc. Earth Planet. Sci.* **7**, 346–349.

Horwell C. J., Williamson B. J., Llewellin E. W., Damby D. E. and Le Blond J. S. (2013) The nature and formation of cristobalite at the Soufrière Hills volcano, Montserrat: implications for the petrology and stability of silicic lava domes. *Bull. Volcanol.* **75**. http://dx.doi.org/10.1007/s00445-013-0696-3.

Hughes H. J., Delvigne C., Korntheuer M., de Jong J., André L. and Cardinal D. (2011) Controlling the mass bias introduced by anionic and organic matrices in silicon isotopic measurements by MC-ICP-MS. *J. Anal. At. Spectrom.* **26**, 1892–1896.

Hurowitz J. A., McLennan S. M., Lindsley D. H. and Schoonen M. A. A. (2005) Experimental epithermal alteration of synthetic Los Angeles meteorite: implications for the origin of Martian soils and identification of hydrothermal sites on Mars. *J. Geophys. Res. Planets* **110**, E07002. http://dx.doi.org/10.1029/2004JE002391.

Hurowitz J. A., McLennan S. M., Tosca N. J., Arvidson R. E., Michalski J. R., Ming D. W., Schroder C. and Squyres S. W. (2006) In situ and experimental evidence for acidic weathering of rocks and soils on Mars. *J. Geophys. Res.* **111**, E02S19. http://dx.doi.org/10.1029/2005JE002515.

Hurwitz S., Goff F., Janik C. J., Evans W. C., Counce D. A., Sorey M. L. and Ingebritsen S. E. (2003) Mixing of magmatic volatiles with groundwater and interaction with basalt on the summit of Kilauea Volcano, Hawaii. *J. Geophys. Res.* **108**, 2028. http://dx.doi.org/10.1029/2001JB001594.

Jones B. F., Eugster H. P. and Reitig S. L. (1977) Hydrochemistry of the Lake Magadi basin, Kenya. *Geochim. Cosmochim. Acta* **41**, 53–72.

Knauss K. G., Bourcier W. L., McKeegan K. D., Merzbacher C. I., Nguyen S. N., Ryerson F. J., Smith D. K., Weed H. C. and Newton L. (1989) Dissolution kinetics of a simple analogue nuclear waste glass as a function of pH, time and temperature. *MRS Proc.* **176**.

Leng M. J., Swann G. E. A., Hodson M. J., Tyler J. J., Patwardhan S. V. and Sloane H. J. (2009) The potential use of silicon isotope composition of biogenic silica as a proxy for environmental change. *Silicon* **1**, 65–77.

Li Y. H., Ding T. P. and Wan D. F. (1994) Experimental study of silicon isotope dynamic fractionation and its geological application. *Miner. Deposit.* **13**, 282–288.

Malin M. C., Dzurisin D. and Sharp R. P. (1983) Stripping of Keanakakoi tephra on Kilauea Volcano, Hawaii. *GSA Bull.* **94**, 1148–1158.

Marin-Carbonne J., Chaussidon M., Boiron M. C. and Robert F. (2011) A combined in situ oxygen, silicon isotopic and fluid inclusion study of a chert sample from Onverwacht Group (3.35 Ga, South Africa): new constraints on fluid circulation. *Chem. Geol.* **286**, 59–71.

Marshall W. L. and Chen C.-T. A. (1982) Amorphous silica solubilities. VI. Postulated sulfate-silicic acid solution complex. *Geochim. Cosmochim. Acta* **46**, 367–370.

Meheut M., Lazzeri M., Balan E. and Mauri F. (2009) Structural control over equilibrium silicon and oxygen isotopic fractionation: a first-principles density-functional theory study. *Chem. Geol.* **258**, 28–37.

Milligan A. J., Varela D. E., Brzezinski M. A. and Morel F. O. M. M. (2004) Dynamics of silicon metabolism and silicon isotopic discrimination in a marine diatom as a function of pCO_2. *Limnol. Oceanogr.* **49**, 322–329.

Minitti M. E., Weitz C. M., Lane M. D. and Bishop J. L. (2007) Morphology, chemistry, and spectral properties of Hawaiian rock coatings and implications for Mars. *J. Geophys. Res. Planets* **112**, E05015. http://dx.doi.org/10.1029/2006JE002839.

Munter P. A., Aepli O. T. and Kossatz R. A. (1947) Hydrofluoric acid–water and hydrofluoric acid–hydrofluosilicic acid–water. *Ind. Eng. Chem.* **39**, 427–431.

Naboko S. I. (1957) A case of gaseous fluorine metasomatism at an active volcano. *Geochemistry* **1957**, 452–455.

Nanyaro J. T., Aswathanarayana U. and Mungure J. S. (1984) A geochemical model for the abnormal fluoride concentration in waters in parts of northern Tanzania. *J. Afr. Earth Sci.* **2**, 129–140.

Oelkers E. H. and Gislason S. R. (2001) The mechanism, rates and consequences of basaltic glass dissolution: I. An experimental study of the dissolution rates of basaltic glass as a function of aqueous Al, Si and oxalic acid concentration at 25 ºC and pH = 3 and 11. *Geochim. Cosmochim. Acta* **65**, 3671–3681.

Oelze M., von Blanckenburg F., Hoellen D., Dietzel M. and Bouchez J. (2014) Si stable isotope fractionation during adsorption and the competition between kinetic and equilibrium isotope fractionation: Implications for weathering systems. *Chem. Geol.* **380**, 161–171.

Oelze M., von Blanckenburg F., Bouchez J., Hoellen D. and Dietzel M. (2015) The effect of Al on Si isotope fractionation investigated by silica precipitation experiments. *Chem. Geol.* **397**, 94–105.

Ohman L. O., Nordin A., Sedeh I. F. and Sjoberg S. (1991) Equilibrium and structural studies of silicon(IV) and aluminum(III) in aqueous solution. 28. Formation of soluble silicic acid–ligand complexes as studied by potentiometric and solubility measurements. *Acta Chem. Scand.* **45**, 335–341.

Opfergelt S. and Delmelle P. (2012) Silicon isotopes and continental weathering processes: assessing controls on Si transfer to the ocean. *Comptes Rendus Geosci.* **344**, 723–738.

Opfergelt S., Cardinal D., Henriet C., Draye X., Andre L. and Delvaux B. (2006) Silicon isotopic fractionation by banana (*Musa* spp.) grown in a continuous nutrient flow device. *Plant Soil* **285**, 333–345.

Opfergelt S., Cardinal D., Andre L., Delvigne C., Bremond L. and Delvaux B. (2010) Variations of $\delta^{30}Si$ and Ge/Si with weathering and biogenic input in tropical basaltic ash soils under monoculture. *Geochim. Cosmochim. Acta* **74**, 225–240.

Pringle E. A., Savage P. S., Badro J., Barrat J.-A. and Moynier F. (2013) Redox state during core formation on asteroid 4-Vesta. *Earth Planet. Sci. Lett.* **373**, 75–82.

Raymo M. E., Ruddiman W. F. and Froelich P. N. (1988) Influence of late Cenozoic mountain building on ocean geochemical cycles. *Geology* **16**, 649–653.

Reynolds B. C., Aggarwal J., Andre L., Baxter D., Beucher C., Brzezinski M. A., Engstrom E., Georg R. B., Land M., Leng M. J., Opfergelt S., Rodushkin I., Sloane H. J., van den Boorn S. H. J. M., Vroon P. Z. and Cardinal D. (2007) An inter-laboratory comparison of Si isotope reference materials. *J. Anal. At. Spectrom.* **22**, 561–568.

Riebe C. S., Kirchner J. W. and Finkel R. C. (2004) Erosional and climatic effects on long-term chemical weathering rates in granitic landscapes spanning diverse climate regimes. *Earth Planet. Sci. Lett.* **224**, 547–562.

Robert F. and Chaussidon M. (2006) A palaeotemperature curve for the Precambrian oceans based on silicon isotopes in cherts. *Nature* **443**, 969–972.

Ruiz-Agudo E., Putnis C. V., Rodriguez-Navarro C. and Putnis A. (2012) Mechanism of leached layer formation during chemical weathering of silicate minerals. *Geology* **40**, 947–950.

Savage P. S. and Moynier F. (2013) Silicon isotopic variation in enstatite meteorites: clues to their origin and Earth-forming material. *Earth Planet. Sci. Lett.* **361**, 487–496.

Savage P. S., Georg R. B., Armytage R. M. G., Williams H. M. and Halliday A. N. (2010) Silicon isotope homogeneity in the mantle. *Earth Planet. Sci. Lett.* **295**, 139–146.

Savage P. S., Georg R. B., Williams H. M., Burton K. W. and Halliday A. N. (2011) Silicon isotope fractionation during magmatic differentiation. *Geochim. Cosmochim. Acta* **75**, 6124–6139.

Savage P. S., Armytage R. M. G., Georg R. B. and Halliday A. N. (2014) High temperature silicon isotope geochemistry. *Lithos* **190**, 500–519.

Seelos K. D., Arvidson R. E., Jolliff B. L., Chemtob S. M., Morris R. V., Ming D. W. and Swayze G. A. (2010) Silica in a Mars analog environment: Ka'u Desert, Kilauea Volcano, Hawaii. *J. Geophys. Res. Planets* **115**, E00D15. http://dx.doi.org/10.1029/2009JE003347.

Shahar A., Ziegler K., Young E. D., Ricolleau A., Schauble E. A. and Fei Y. W. (2009) Experimentally determined Si isotope fractionation between silicate and Fe metal and implications for Earth's core formation. *Earth Planet. Sci. Lett.* **288**, 228–234.

Stefurak E. J. T., Fischer W. W. and Lowe D. R. (2015) Texture-specific Si isotope variations in Barberton Greenstone Belt cherts record low temperature fractionations in early Archean seawater. *Geochim. Cosmochim. Acta* **150**, 26–52.

Steinhöfel G., Horn I. and von Blanckenburg F. (2009) Micro-scale tracing of Fe and Si isotope signatures in banded iron formation using femtosecond laser ablation. *Geochim. Cosmochim. Acta* **73**, 5343–5360.

Steinhöfel G., von Blanckenburg F., Horn I., Konhauser K. O., Beukes N. J. and Gutzemer J. (2010) Deciphering formation processes of banded iron formations from the Transvaal and the Hamersley successions by combined Si and Fe isotope analysis using UV femtosecond laser ablation. *Geochim. Cosmochim. Acta* **74**, 2677–2696.

Tosca N. J., McLennan S. M., Lindsley D. H. and Schoonen M. A. A. (2004) Acid-sulfate weathering of synthetic Martian basalt: the acid fog model revisited. *J. Geophys. Res. Planets* **109**, E05003. http://dx.doi.org/10.1029/2003JE002218.

van den Boorn S. H. J. M., van Bergen M. J., Vroon P. Z., de Vries S. T. and Nijman W. (2010) Silicon isotope and trace element constraints on the origin of similar to 3.5 Ga cherts: implications for early Archaean marine environments. *Geochim. Cosmochim. Acta* **74**, 1077–1103.

White A. F. and Hochella M. F. (1992) Surface chemistry associated with the cooling and subaerial weathering of recent basalt flows. *Geochim. Cosmochim. Acta* **56**, 3711–3721.

Young E. D., Galy A. and Nagahara H. (2002) Kinetic and equilibrium mass-dependent isotope fractionation laws in nature and their geochemical and cosmochemical significance. *Geochim. Cosmochim. Acta* **66**, 1095–1104.

Ziegler K., Chadwick O. A., Brzezinski M. A. and Kelly E. F. (2005) Natural variations of $\delta^{30}Si$ ratios during progressive basalt weathering, Hawaiian islands. *Geochim. Cosmochim. Acta* **69**, 4597–4610.

Ziegler K., Young E. D., Schauble E. A. and Wasson J. T. (2010) Metal-silicate silicon isotope fractionation in enstatite meteorites and constraints on Earth's core formation. *Earth Planet. Sci. Lett.* **295**, 487–496.

Associate editor: Clark M. Johnson